Bio-Inspired Trailing Edge Noise Control

Ian A. Clark[1], W. Nathan Alexander[2] and William Devenport[3]
Center for Renewable Energy and Aerodynamic Testing,
Virginia Polytechnic Institute and State University, Blacksburg, Virginia 24061

Stewart Glegg[4]
Florida Atlantic University, Boca Raton, Florida 33431

Justin W. Jaworski[5]
Lehigh University, Bethlehem, Pennsylvania 18015

Conor Daly[6] and Nigel Peake[7]
University of Cambridge, Cambridge CB3 0WA, UK

Strategies for trailing edge noise control have been inspired by the downy canopy that covers the surface of exposed flight feathers of many owl species. Previous wind tunnel measurements demonstrate that canopies of similar characteristics can reduce pressure fluctuations on the underlying surface by as much as 30dB, and significantly attenuate roughness noise generated by that surface. In the present work, surface treatments are designed to replicate the effects of the canopy in a form suitable for application to an airfoil. These treatments are installed directly upstream of the trailing edge to modify the boundary layer turbulence prior to acoustic scattering by the edge. Over 20 variants of these designs have been tested by performing aeroacoustic wind tunnel measurements on a tripped DU96-W180 airfoil at chord Reynolds numbers of up to 3 million. Compared to the unmodified airfoil, the treatments provided up to 10dB of broadband attenuation of trailing edge noise. The effectiveness of the treatment is not highly dependent on a particular geometry, but there appears to be strong potential for optimization. The surface treatments remain effective over

[1] Graduate Student, Department of Aerospace and Ocean Engineering, Student Member AIAA.
[2] Assistant Professor, Department of Aerospace and Ocean Engineering, AIAA Member.
[3] Professor, Department of Aerospace and Ocean Engineering, Associate Fellow AIAA.
[4] Professor, Department of Ocean and Mechanical Engineering, Associate Fellow AIAA.
[5] Assistant Professor, Department of Mechanical Engineering and Mechanics, Senior Member AIAA.
[6] Research Associate, Department of Applied Mathematics and Theoretical Physics.
[7] Professor, Department of Applied Mathematics and Theoretical Physics, Member AIAA.

an angle of attack range that extends over 9 degrees from zero lift. Aerodynamic impact of the treatment appears minimal.

I. Introduction

THIS paper describes an experimental study aimed at trailing edge noise control strategies inspired by the unique features found on the wings of owls that use acoustic stealth while hunting prey [1, 2, 3]. These features include a comb of evenly-spaced bristles along the wing leading-edge, a porous and elastic trailing edge fringe, and fine downy hairs that coat the exposed surfaces of the flight feathers. Geyer *et al.* [4] sought to relate the fine downy coating to porosity of the wing by performing experiments involving aerodynamic and acoustic testing of airfoils manufactured entirely of porous material. Their results showed that porous airfoils can be effective for trailing edge noise reduction. However, the amount of noise reduction seemed to be a complex function of the resistivity of the material, and the aerodynamic performance suffered as resistivity decreased (i.e., as porosity increased). Jaworski and Peake [5, 6] analyzed the trailing edge condition and found that both porosity and flexibility weaken the well-known fifth-power dependency of the radiated acoustics of a trailing edge, with the greatest reduction in edge amplification occurring when these characteristics are combined. However, Jaworski and Peake [5, 6] did not consider the effect of the downy hairs on the upper-wing surface. The purpose of this study is to investigate the importance of the downy hairs on the radiated noise and to develop noise control strategies that are inspired by their features.

The work described in this paper follows on from the study of Clark *et al.* [7], which considered the potential of a hairy surface to suppress noise generated by roughness lying underneath. It was shown that the downy hairs of the owl grow nearly perpendicular from the feather surface, but then lean over to form a canopy suspended about 0.5 mm above the feather substrate, with an open area ratio of about 70% (Fig. 1). Wall-jet wind tunnel experiments were performed to examine the aeroacoustic effects of artificial canopies designed to mimic the effects of a canopy of this open area ratio on the surface pressure fluctuations and roughness noise generated by an underlying rough surface. Efforts included shrouding surfaces using canopies constructed from materials of the type used for wedding veils (Fig. 2a) and a series of canopies constructed using large numbers of parallel fibers, oriented in the flow direction just above the flow surface (Fig. 2b).

Measurements of surface pressure fluctuations underneath these canopies and of the roughness noise generated by surfaces shrouded by these canopies produced some surprising results. Even though the canopies had high open area

ratios of about 70% they attenuated surface pressure fluctuations underneath them by as much as 30 dB. The canopies were also found to attenuate broadband roughness noise, presumably because roughness noise is caused by the surface pressure fluctuations [8].

These unexpected findings spawned a new line of inquiry when it was realized that such a large reduction in surface pressure fluctuations might also serve to attenuate trailing edge noise if a treatment replicating the effects of the canopy could be designed that was suitable for application to an airfoil. This paper describes an experimental study of a series of treatments inspired by this idea. An extensive series of wind tunnel tests have been performed on a wind turbine airfoil at Reynolds numbers comparable to full scale. Measurements of the sound radiated by the airfoil trailing edge have been made both for the clean airfoil and with an extensive series of trailing edge treatments inspired by the owl down and the results of Clark *et al.* [7]. The effects of a broad range of treatment parameters were studied. We find that the treatment produces a broadband reduction in trailing edge noise levels of up to 10 dB. The treatment remains surprisingly effective throughout a wide parameter range and is not highly dependent on a particular geometry, but there appears to be strong potential for optimization. The treatment is effective over an angle of attack range that extends to over 9 degrees from the zero lift condition.

II. Apparatus and Instrumentation

A. Stability Wind Tunnel

All tests were performed in the Virginia Tech Stability Wind Tunnel. This facility is a continuous, single return, subsonic wind tunnel with 7.3-m long removable rectangular test sections of square cross section 1.85 m on edge. The general layout is illustrated in Fig. 3.

The tunnel is powered by a 0.45-MW variable speed DC motor driving a 4.3-m diameter propeller that provides a maximum speed in the test section (with no blockage) of about 80 m/s. Ahead of the test section, flow is directed into a 5.5×5.5-m^2 settling chamber containing 7 turbulence-reducing screens each with an open area ratio of 0.6 and separated by 0.15 m. Flow exits this chamber through the 9:1 contraction nozzle which further reduces turbulence levels and accelerates the flow to test speed as it enters the test section (Fig. 4).

Flow through the empty test section is both closely uniform and of very low turbulence intensity. Table 1 shows measurements from 2006 of free stream turbulence levels as a function of flow speed. Turbulence levels are as low as 0.016% at 12 m/s and increase gradually with flow speed. Choi and Simpson [9] measured the lateral integral scales

of the streamwise velocity in both the horizontal L_z and vertical L_y directions. They found L_z=56 mm for 15 m/s and 28 mm for 37.5 m/s, and L_y=122 mm for 15 m/s and 25 mm for 37.5 m/s.

Figures 4 and 5 detail the Stability Wind Tunnel aeroacoustic test section used in the present study. This test section has acoustically treated lower and upper walls, consisting primarily of Kevlar-covered metal perforate panels backed by 0.45-m sound absorbing foam wedges. The central 4.2-m length of both side walls are made from Kevlar panels placed under tension. The Kevlar contains the vast bulk of the flow, and is almost transparent to sound [10]. Sound generated by a model placed at the center of the test section can therefore propagate out of the flow and into anechoic chambers placed on either side of the test section. These chambers, lined with 0.61-m foam wedges, are anechoic down to 190 Hz. The 4.2-m long, 2.6-m deep and 3-m high interior volume of the chambers allows for the placement of acoustic instrumentation. This unusual arrangement has a number of advantages over a conventional free-jet tunnel. It eliminates the need for a jet catcher, reduces aerodynamic interference corrections by about a factor of 4, allows for a long test section that provides a clear separation between model generated sound and the parasitic noise of the facility, and permits acoustic instrumentation to be placed close to the model, yet out of the flow. Further details of the facility and its calibration are given by [10]. Acoustic and aerodynamic corrections applied to measurements made in this test section are also described by [10].

B. Airfoil model, boundary-layer tripping, and lift measurement

The 0.8-m chord airfoil model used for the experiments is illustrated in Fig. 4, as installed in the test section. The model has a DU96-W180 section – a standard wind turbine blade profile with a maximum thickness of 18% chord. The model was assembled from 50.8-mm thick laminates, each cut with the airfoil profile. The laminate construction allows for easy installation of internal instrumentation, while careful alignment and accurate machining of the laminates ensures a smooth and continuous airfoil surface.

Serrated tape (Glasfaser-Flugzeug-Service GmbH 3D Turbulator Tape) of thickness 0.5 mm was used to trip the airfoil boundary layers. The tape was applied at the 5% and 10% chord locations of the suction and pressure sides of the airfoil, respectively.

Pressure distributions and lift on the model were measured using some 80 1-mm pressure taps distributed around the profile. Pressures were sensed using Esterline 9816/98RK pressure scanners with a range of ±2.5 psi (rated accuracy of ±0.05% full scale) connected to the pressure taps through 1.6-mm Tygon tubing.

C. Measurement of drag and reference conditions

Tunnel free-stream velocity was monitored using the pressure difference between static taps located in the walls of the wind tunnel settling chamber and contraction, sensed using the Esterline 9816/98RK pressure scanner system. Temperature in the test section was monitored using an Omega Thermistor type 44004 (accuracy ±0.2°C) and the ambient absolute pressure was determined using a Validyne DB-99 Digital Barometer (resolution 0.01" Hg).

For some conditions a rake of Pitot and static probes was used to measure profiles through the airfoil wakes and infer the drag using a momentum balance approach. The rake consists of 113 1.6-mm diameter Pitot probes and 7 Pitot-static probes distributed over a 1.8-m length. Mounted on the rake system are four DTC Initium ESP-32HD 32-channel pressure scanners with a range of ±2.5 psi and a rated accuracy of ±0.03% to which the tubes are connected. The rake is acoustically noisy and was therefore not used during sound measurements.

D. Sound measurement

Airfoil trailing edge noise was measured using a phased array system located in the port-side anechoic chamber facing the suction side of the airfoil, Fig. 4a. The array has 117 Panasonic electret microphones type WM-64PNT arranged in 9 spiral arms mounted on a solid 1.1-m diameter carbon-fiber disk. These microphones have a flat frequency response from 20-16000 Hz. The array was calibrated to within ±5° phase and 0.4 dB amplitude from 500 Hz to 16000 Hz. The array was mounted in the port side chamber which was the suction side of the airfoil slightly upstream of the quarter-chord position. Boundary layer refraction effects, convective effects, pressure doubling due to the microphones being mounted on a solid surface, and attenuation through the Kevlar cloth have all been accounted for in post-processing. Data were recorded simultaneously at 51200 Hz for 32 seconds with two 64 channel PCI-based data acquisition cards. The signals were processed through an anti-aliasing filter with a cut-off frequency of 20 kHz. Spectral quantities were computed by averaging the Fourier transform of blocks of 8192 samples. The diagonal of the cross-spectrum was removed in order to omit uncorrelated noise in the beamformed maps. Integrated spectra were computed by integrating the beamformed results over a selected region.

E. Trailing edge noise treatments

Two different treatment designs were developed with the goal of replicating the effects of a canopy on reducing surface pressure fluctuations, seen in the wall-jet tunnel measurements of Clark *et al.* [7], in a form suitable for application to an airfoil in external flow. The designs are illustrated in Fig. 6 and are referred to as finlet fences and

finlet rails. A total of 20 variants on these designs were fabricated using rapid prototyping. All design variants involved either the rail or fence treatment beginning 101.6 mm upstream of the trailing edge (87.3% chord), and in all cases the treatment was supported on a thin sheet of material (the substrate) glued to the airfoil, with its leading edge placed 114.3 mm upstream of the airfoil trailing edge (85.7% chord). Only the middle half-span of the airfoil was treated (see Fig. 4b). The leading edge of the substrate was, in all cases, faired to the airfoil surface by covering it with 0.1-mm thick metal tape.

The upper edges of finlet fences (Fig. 6a) are designed to present the same geometry to the airfoil boundary layer flow as the unidirectional canopy of Fig. 2b. A total of 14 such fence configurations were tested, including variations in finlet spacing, height, thickness, extension past the trailing edge, and substrate thickness. The rails (Fig. 6b) more explicitly replicate the fiber geometry of the canopy in Fig. 2b, with streamwise cylindrical elements mounted from the surface using periodic swept supports. A total of 6 such configurations were tested. Table 2 shows the full test matrix for both types of configurations. The table also includes the control cases, including the untreated tripped airfoil and two cases in which only substrate layers were applied to the airfoil surfaces.

As a final point, an important distinction should be emphasized here to differentiate the present treatment from "riblets", which have some shape similarities to finlets used for viscous drag reduction [11, 12]. Riblets act on the very near wall boundary layer structure and have a typical height and spacing of 10 to 15 wall units. Finlets are of a different scale altogether (10 to 100% of the boundary layer thickness) and are designed to reduce noise by acting on the boundary layer turbulence as a whole.

III. Results and Discussion

Measurements were made at flow speeds 50 and 60 m/s, corresponding to chord Reynolds numbers of 2.5 and 3.0 million, respectively. We present here only results for Reynolds number 3.0 million, since those measured at 2.5 million are almost identical. For all cases the airfoil boundary layers were fully turbulent, having been tripped as described in section II.B. For all finlet fence and finlet rail configurations tested, far-field sound and mean surface pressure (and therefore lift) measurements were made with the airfoil pitched from -4 to 16 degrees geometric angle of attack in approximately two-degree increments. This range encompasses zero lift ($\alpha \approx -2.5°$) as well as stall ($\alpha \approx 11°$). Aerodynamic corrections [10] were used to calculate the effective angle of attack corresponding to each geometric angle of attack. All data will be presented in terms of these effective angles. In all cases, a measurement sequence

with a treated condition was immediately followed or preceded by a measurement of the untreated condition to minimize the experimental uncertainty between the two and to establish (by comparing the many untreated-condition measurements) the repeatability of the results. Thus, the wind tunnel entry included many repeat measurements of configuration C0, which will be referred to as the 'clean condition'. Configuration F8 was also repeated so that drag measurements could be made with the rake system without interference of the acoustic measurement. As the majority of noise reduction was observed in the frequency range of 1500 – 5000 Hz, Table 3 shows overall levels in this frequency range for each configuration for which spectra are presented.

A. Noise measurements made with the clean airfoil

Figures 7 and 8 summarize the trailing edge noise measurements made with the clean airfoil at Re = 3 million. Figure 7 shows sample beamform maps at 3 kHz. All acoustic source maps are shown on a dB scale with a 10 dB range, using a reference pressure of 20 μPa. Figure 8 compares noise spectra integrated over the central 25% of the blade span, as indicated by the dashed box shown in Fig. 7(a). Starting at the zero lift angle of attack (Fig. 7a) the trailing edge noise is clearly detectable at this frequency and is seen to form a clean uniform band along the trailing edge. At 3 kHz, as the angle of attack is increased, the trailing edge noise actually decreases slowly (note the change in the absolute level of the color scales in Fig. 7) so that, once the quietest angle of attack of 3 degrees is reached, the spurious lobes associated with the background noise levels generated by the facility appear more prominently. The trailing edge noise is still easily distinguished, however, and remains so through 6.9 degrees angle of attack until the airfoil stalls. At stall, airfoil generated noise levels greatly increase (e.g. Fig. 7e) and a stall pattern with two spanwise cells is formed, clearly visible in the beamform map. Note that the weak source near the leading edge in Figs. 7(c) and 7(d) is believed to be background facility noise scattered from the leading edge.

One-12th octave band integrated spectral levels for angles of attack of -2.5, -0.5, 3.0, 6.9, and 14.8 degrees are compared in Fig. 8. The area of integration for this and subsequent similar figures is shown by the black box drawn on Fig. 7(a). Results are presented only up to 5 kHz as above this frequency, background noise makes it difficult to distinguish trailing edge noise. The difference in trailing edge noise levels for varying angles of attack only becomes distinguishable above about 1500 Hz. This difference may be partly due to the beamwidth of the phased array which becomes comparable to the integration area at this frequency as will be discussed further below. Above 1500 Hz the sound spectra are seen to be broadband in all cases. The sound level variations with angle of attack observed at 3 kHz

in the beamform maps are seen to be representative of the whole frequency range, with spectral levels lowest at 3 degrees angle of attack where they are up to 7 dB lower than those seen at zero lift.

B. Effects of the baseline fence treatment

We examine first the effects of the baseline airfoil treatment, which we take as configuration F0. The treatment, shown in Fig. 9, consists of 0.5 mm thick fences with a maximum height of 4 mm spaced every 4 mm across the span. The fences extend by 10 mm past the trailing edge and are attached to the airfoil via a 0.5 mm thick substrate. The treatment was placed on both sides of the airfoil and covered the center half-span of the model, so that direct comparisons could be drawn with the untreated regions at the ends of the airfoil. Figure 10 shows measurements of the lift on the airfoil as a function of angle of attack. There appear to be no detrimental effects of the treatment on the lift, and, indeed, it appears that the lift is slightly enhanced post stall. Note that lift measurements were integrated using pressure distributions measured over the first 85% of the airfoil chord, extrapolated around the trailing edge using the Kutta condition requirement, since the last 15% of the chord was covered by the treatments when they were applied. This methodology was checked by comparing integrated lift results from the untreated airfoil using both the full set of pressure taps, and the taps on the first 85% of chord (as if the airfoil were treated). No significant difference was found between the results obtained by using the two different sets of pressure taps.

Figure 11 shows beamform maps for the treated airfoil at Re=3 million for the unstalled angles of attack (the treatment had no discernable influence on the airfoil sound, either positive or negative, post-stall). Integrated spectra for the treated and untreated airfoil are compared for the zero lift angle of attack in Fig. 12, and for other sample angles of attack in Fig. 13. At the zero lift angle of attack (Fig. 11a) the beamform map shows no discernable trailing edge noise coming from the treated portion of the airfoil, whereas the untreated portions appear almost unaltered from the results shown in Fig. 7(a). This indicates about a 10 dB attenuation at 3 kHz for this condition. It should be noted here that, because of the significant attenuation of the noise in the trailing edge region by the finlets, it is possible that some remaining noise in this region is actually due to side lobes of other nearby sources, such as the untreated portion of the airfoil, or to background noise from the facility. As such, the 10 dB attenuation seen here could be considered a conservative estimate. As the angle of attack increases (Fig. 11(b) through (d)) the effectiveness of the treatment diminishes but is still substantial at -0.5 and 3 degrees angle of attack and is certainly still detectable at 6.9 degrees.

Figure 12 shows the effectiveness of the treatment over a broader range of frequencies at the zero lift condition (α=-2.5°). The attenuation achieved by the treatment is clearly broadband with reductions between 5 and 10 dB for

frequencies between 2 kHz and 5 kHz. For frequencies below 2 kHz, the effectiveness of the treatment appears to diminish, ultimately disappearing at about 1400 Hz. However, this is at least partly an artificial effect of the diminishing ability of the array to focus as the frequency is reduced. To illustrate this, Fig. 12 includes thumbnail images showing beamform maps of the treated airfoil sound field at different frequencies. Each thumbnail has been centered on the frequency to which it refers. At about 1500 Hz the beamwidth of the array, defined as the width of the area 3 dB below the maximum of the main lobe of the point spread function, is approximately 0.5 m. This is comparable to the width of the treated portion of the airfoil span, and thus the lobes associated with the untreated portions at the two ends of the airfoil have begun to merge. There still appears to be some attenuation of the sound between the untreated regions, but this attenuation is largely obscured by blurring of the beamform map. As the frequency is reduced to 1 kHz, the ability of the array to distinguish features on the scale of the treated portion of the span has been completely lost. In an effort to reduce the ambiguity of low-frequency results due to the array characteristics, the CLEAN-SC deconvolution algorithm [13] was used in an attempt to extract information at low frequencies without success. CLEAN-SC works well for incoherent isolated sources, but performs poorly for a distributed line source like considered here, therefore, results were obscured by misplaced sources and facility noise.

The broadband effectiveness of the treatment is illustrated for a set of unstalled angles of attack in Fig. 13. At -0.5 degrees angle of attack the attenuation achieved with the treatment above 2 kHz is between about 3 and 7 dB. At 3 degrees, the effectiveness of the treatment is somewhat diminished at frequencies below about 3.5 kHz, but is enhanced at higher frequencies, reaching about 12 dB near 4 kHz. At 6.9 degrees angle of attack the effectiveness of the treatment is noticeably reduced, but significant reductions in sound, of up to about 3 dB, are still visible at frequencies over 2.5 kHz. At no angle of attack is the treatment seen to have any detrimental effect on the radiated sound.

It is important to recognize that the substrate is not an inactive component of the treatment. Figure 14 shows the effect on integrated acoustic levels of adding only a 0.5 and a 0.75 mm thick substrate to the airfoil, as compared to the clean case. (Note that configuration F0 is mounted on the thin, 0.5 mm substrate.) At α=-2.5° and -0.5° the substrate adds to the trailing edge noise at around 1500 Hz and 1800 Hz for the 0.75 mm and 0.5 mm thicknesses respectively, quite possibly because of vortex shedding enhanced because of the substrate adding to the trailing edge thickness. At the same time, sound levels with the substrates are somewhat lower (by up to 5 dB for the 0.5 mm and 7 dB for the 0.75 mm) at higher frequencies. This could be because of a nonlinear redistribution of energy into the lower-frequency

vortex shedding motions. At α=3° and 6.9° the increased levels ascribed to vortex shedding are smaller or absent. At the same time the noise reductions are also smaller and do not appear until higher frequencies.

At the very least, the fences are clearly suppressing the detrimental effects of the substrate at low frequencies while enhancing the noise reduction at high frequencies. One possible explanation is that the finlets suppress the surface pressure fluctuations at the airfoil trailing edge, and also coherent vortex shedding here by breaking up the spanwise correlation length scale of the boundary layer. One can imagine the unidirectional canopy of [7] reducing wall pressure fluctuations by a similar mechanism.

C. Effects of the fence parameters

In this section we examine the effects of varying the fence parameters. Note that all the treated cases produced lift characteristics that are almost identical to those of configuration F0, i.e. the same as, or slightly better than, the untreated airfoil. Figure 15 shows the effects of changing the fence spacing by comparing integrated sound levels from configurations F2, F0, F3, and F4 representing spacings of 1, 4, 6 and 10 mm. Photographs showing three of these four treatments are shown in Fig. 16.

Overall, the noise spectra appear to show a clear progression with fence spacing for angles of attack α= -2.5°, -0.5° and 3°. At these conditions, the 6-mm spacing produces similar noise reductions to the 4-mm spacing described above. Reductions with the 10-mm spacing are less, particularly at frequencies over 3.5 kHz. Reductions with the 1-mm spacing are greater, by 1-4 dB over almost all the frequency range. This dependence appears consistent with the fences limiting the spanwise correlation length scale – the smaller the spacing, the smaller the maximum correlation scale that can survive to the trailing edge. There is clearly a limit to the beneficial effect though, in the form of the intense spike that appears in the spectra for the 1-mm spaced fence at around 650 Hz. At 60 m/s, this frequency corresponds to a distance scale of about 18 mm (at a Strouhal number of 0.2), which is of the same order as the sum of the trailing edge thickness (2.5 mm), both substrate layers (1 mm) and two fence heights (8 mm). The implication is that below a certain minimum spacing, somewhere between 1 and 4 mm in this case, the fences start to behave like a solid, much thicker, blunt trailing edge. At α=6.9° the noise reductions are smaller in all cases, and the dependence on fence-spacing less apparent. Acoustic levels at this angle of attack are slightly lower at high frequencies with the 6-mm spaced fence (configuration F3), perhaps because the substrate used with this configuration was slightly thicker than for the other cases in this comparison (0.75 versus 0.5 mm).

The effects of extending the treatment past the trailing edge are examined in Fig. 17. This compares integrated noise spectra for case F2 (1-mm spaced, 4-mm high fences extending 10 mm past the trailing edge) to case F1 (identical geometry but shortened so that the fences end at the trailing edge). At lower angles of attack, α= -2.5° and -0.5° both configurations produce almost identical acoustic results, including the intense vortex shedding peak associated with the 1-mm spacing. The results are also quite similar at 3° and 6.9° angles of attack except that high frequency noise levels (>3 kHz) are noticeably lower without the extension. It appears, therefore, that the extension offers little if any benefit and, indeed, comes at a price at higher angles of attack. This implies that the fence 'finlets' are, as hypothesized, manipulating the boundary layer structure as it reaches the trailing edge, rather than altering the scattering efficiency by reshaping the trailing edge, as is accomplished by a trailing edge serration or comb. This suggests it may be possible to maximize noise attenuation by combining both control strategies.

Figure 18 examines the effect of fence height on the acoustic signature of the airfoil. Here results for configuration F0 (4-mm high, 4-mm spaced, fences) are compared to those of configuration F8 (8-mm high, 4-mm spaced, fences) and the clean airfoil. At all angles of attack and at almost all frequencies, noise levels are reduced by 1 to 2 dB by a doubling of the fence height. This effect can be understood in the context of the boundary layer thickness at the trailing edge. XFOIL [14] calculations suggest displacement thicknesses, for the tripped DU96 at Re=3 million, of 0.9, 1.2, 1.8 and 3.1 mm for the suction side and 0.7, 0.5, 0.3, and 0.2 mm for the pressure side at α=-2.5°, -0.5°, 3°, and 6.9° respectively.

Assuming overall boundary layer thicknesses five to ten times these values, it is clear that increasing the fence height from 4 to 8 mm would cause the fences to cut substantially more of the boundary layer, particularly on the suction side, and thus have a greater impact on the spanwise correlation length scale and thus the radiated noise. This conceptual model implies that further noise reductions at high angle of attack could be achieved by increasing the height of the suction side fences, in accordance with the increase in boundary layer thickness.

Unlike other configurations, the 8-mm high fence treatment of configuration F8 was tested twice, the second time with the drag rake system in place. Figure 19 compares the drag on the airfoil with this treatment, with that of the clean case (configuration C0) and of the corresponding substrate alone case (configuration C1). The clean airfoil exhibits a drag bucket with a minimum C_d of about 0.008 near the zero-lift angle of attack of -2.5°. The drag then rises gradually with angle of attack through an angle of attack of 8° after which the airfoil stalls resulting in erratic fluctuations in the drag curve and overall a sudden rise. (Note that the slight reduction in C_d between 8° and 11° is a

consequence of basing the drag on a wake measurement at a single spanwise station – three dimensional flow at the initiation of stall can result in a local thinning of the wake, despite its overall dramatic growth.) Adding the substrate to the airfoil (configuration C1) has no significant impact on the unstalled drag. Adding the 8-mm high fences of configuration F8 increases the drag by about 10%. The airfoil has a surface area of some 6400 square millimeters for every 4 mm of span. The fences add about 500 square millimeters to this total, or about 8%, indicating that, to the accuracy of its measurement, the increase in wetted surface area associated with the fences accounts for the drag increase.

Configuration F9 replicates the fence geometry of configuration F0, but with 2-mm thick fences in place of 0.5-mm thick fences and with a 0.75-mm thick substrate in place of a 0.5-mm thickness, as shown in Fig. 20. The effects of these changes on the sound measured above the suction side of the airfoil are shown in Fig. 21. Above 1.5 kHz the effects of these geometry changes is a slight reduction (up to about 3 dB) of acoustic levels. Some fraction of these could, perhaps, be ascribed to the substrate effect (Fig. 14), but at the very least we see that the thicker fences are not detrimental to the acoustic performance of the treatment. The results below 1.5 kHz are less clear. At the lower angles of attack, acoustic levels appear suppressed by the thicker treatment around 1100 Hz, but these levels are increased by the treatment at around 700 Hz, perhaps indicating that the fences initiate some organized turbulent motion at these low frequencies.

Figure 22 shows the effects of only using the configuration F8 treatment on the suction side of the airfoil (configuration F8S) versus the treatment on both sides (configuration F8). In both cases the treatment is 8-mm high fences with a spacing of 8 mm. At angles of attack of -2.5°, -0.5° and 3° the effect of removing the pressure side treatment is, to a good approximation, to halve the decibel attenuation produced by the treatment. It is difficult to draw a solid quantitative inference from this result, since it is unclear how much of the sound is generated by the suction and pressure side boundary layers, and by the interaction between them. However, if we assume equal contributions from both boundary layers and no interaction effect, then a complete elimination of the sound from the suction side boundary layer would be observed as a broadband 3 dB reduction relative to the clean airfoil. At 6.9 degrees angle of attack the removal of the pressure side treatment has no effect on the sound radiated from the foil. This suggests that either the pressure-side treatment is ineffective at large angles of attack or, as seems more probable, the suction-side boundary layer is the dominant contributor to the far-field sound at such conditions.

D. Effects of the rail treatments

In addition to the finlet designs discussed above, a series of tests were carried out on rails that extend from the surface, as shown in Figure 6. These shapes are more like the hairs on the owl wing discussed in section I. Figure 23 shows the first rail case, configuration R0, installed on the trailing edge portion of the airfoil trailing edge region. This configuration uses 1.25-mm diameter rails rising to 4 mm above the airfoil surface and spaced at 2.5-mm intervals across its span. The rails extend 10 mm downstream of the trailing edge. In terms of aerodynamic performance, all the rail cases produced lift curves almost indistinguishable from those of configuration F0, shown in Fig. 10. Drag measurements were not made with the rail cases.

The geometric parameters of configuration R0 do not exactly match any of the fence cases but fall somewhere between configuration F2 (4-mm high fences with 1-mm spacing) and configuration F0 (4-mm high fences with 4-mm spacing). Noise measurements made with configurations R0, F2 and F0 are compared with those for the clean airfoil in Fig. 24. At angles of attack of -2.5°,-0.5°, and 3° the rail treatment produces almost identical noise attenuation to the 4-mm spaced fences, and, unlike the 1-mm spaced fences, there is no evidence of low frequency vortex shedding associated with an effective increased trailing edge thickness. Close to stall, however, at an angle of attack 6.9° the rails perform significantly better than the fences producing detectable attenuation at frequencies down to 2 kHz and doubling the dB attenuation at higher frequencies.

The acoustic performance of a selection of the other rail cases is plotted in Fig. 25. This includes elimination of the trailing edge extension (configuration R1), doubling of the maximum rail height to 8 mm (configuration R2) and doubling of the diameter and spacing to 2.5 mm and 8 mm respectively (configuration R3). The change that has the least effect appears to be the elimination of the trailing edge extension which has no impact on the sound attenuation compared to configuration R0 other than, perhaps, a slight reduction in attenuation at the very highest frequencies. As with the fence configurations, increasing the spacing (configuration R3), reduces the attenuation achieved by the treatment by a few dB above about 2500 Hz. Contrary to what was seen with the fences, doubling the maximum height of the rails to 8 mm (compare configurations R0 and R3) is actually counter-productive particularly at the highest angle of attack (6.9°) where the additional height might expect to be beneficial in penetrating the thicker suction side boundary layer. It may be that, if made too large, the space under the rails may permit reconnection of spanwise coherent structures and thus limit the reduction in spanwise correlation length scale that can be achieved.

IV. Concluding Remarks

Airfoil treatments to reduce trailing edge noise, inspired by the downy canopy found to coat the flight feathers of some owls, have been developed. These treatments were designed to replicate the surface-pressure-attenuating effects of the canopy in a form suitable for application to an airfoil.

Over 20 variants of these designs have been tested by performing aeroacoustic wind tunnel measurements on a tripped DU96-W180 airfoil at chord Reynolds numbers up to 3 million. Variations include treatment thickness, density, length, position relative to the trailing edge, and the effectiveness of treating only one side of the trailing edge. Compared to the untreated airfoil, the treatments were found to be effective at providing broadband attenuation of trailing edge noise of up to 10 dB. Treatments were found to be effective over an angle of attack range that extends to over 9 degrees from the zero lift condition. Airfoil treatments were observed to have no detrimental effect on the lift performance of the airfoil. Drag is slightly increased but only by an amount commensurate with the increase in wetted surface area associated with the treatment.

The acoustic level attenuation is found to be robust to changes in non-dimensional flow parameters, and there appears to be good potential for tailoring the treatment to suit engineering system design requirements. The changes in noise attenuation in response to changes in geometric parameters of the finlet fence treatment provide the best clues about how this could be accomplished. From decreased performance with increased finlet spacing, along with increased performance with increased finlet height, it is reasonable to conclude that the extent to which the finlets can cut, deform, or otherwise decorrelate the turbulent structures in the boundary layer is the primary driver in the noise attenuation mechanism. However, it is important to limit the effect of the treatment on the mean flow, as demonstrated by the increased low-frequency noise produced by the 1-mm spaced finlets attributed to vortex shedding. The assertion that the finlets are acting to modify the scattering edge in a manner similar to serrations or combs is refuted by the observation of improved performance when the finlets do not extend past the trailing edge. This observation suggests some possibilities for improved performance. One option is to shift the finlets upstream of the trailing edge, in which case finlets of a given size will encompass a higher portion of the boundary layer and therefore have a greater effect on the turbulence there. Alternatively, the use of smaller finlets upstream could lead to decreased drag compared to the use of larger finlets near the trailing edge due to the decreased additional wetted area. It should be noted here that this option assumes the decorrelation of spanwise turbulent structures by the finlets persists over a significant portion of the chord of the airfoil downstream of the finlets, and that this length is less than that between the end of the finlet

and the trailing edge. The second possibility is to combine the finlet treatment with modifications to the trailing edge geometry, such as the aforementioned serrations or combs, with the intent of combining both boundary layer pre-treatment and decreased efficiency of the scattering edge.

The finlet rail performance trends offer additional clues about the relevant flow physics around the treatments. Doubling the height of the rails appeared to decrease performance, particularly at higher frequencies where the sound is produced by smaller turbulent eddies in the boundary layer. This trend may suggest that the increased open area beneath the rails prevents the smaller scale turbulent fluctuations from being decorrelated (one could imagine the open space allowing pressure and velocity fluctuations to be communicated or propagated beneath the rails). The additional high-frequency noise above that of the untreated case may be caused by increased turbulence levels generated by the flow past the rails (which have a cylindrical cross-section).

In contrast to the information provided by changing geometric parameters of the treatment, the acoustic effects of adding the substrate only serve to complicate and obscure the effects of the treatment itself. However, it can be reasonably concluded that, although the substrate has a significant influence on the acoustics when placed on its own, the effect of the finlets dominates over this influence when the full treatment is applied. The additional noise (compared to the untreated airfoil) observed at some frequencies due to the substrate is completely eliminated by the finlets. At frequencies where the substrate showed a noise reduction compared to the untreated airfoil, the finlets improved and increased this noise reduction even further. The only remaining concern is whether or not the finlets might be somehow dependent on the substrate for most of the noise reduction. One could imagine the upstream step of the substrate exerting an influence on the boundary layer such that a certain flow pattern was set up, perhaps featuring an additional bias towards larger, more spanwise-oriented turbulent eddies. The finlets might then have a greater influence on this new flow than, say, the unmodified boundary layer over the clean airfoil. This seems unlikely, however, considering the difference in scales between the substrate thickness (0.5 mm), finlet height (4 or 8 mm), and the boundary layer thickness (on the order of 10 to 20 mm on the airfoil's suction side).

Acknowledgments

The authors would like to thank the Office of Naval Research, in particular Drs. Ki-Han Kim and Woei-Min Lin, for their support under grants N00014-13-1-0244, N00014-14-1-0242, and N62909-12-1-7116 (NICOP). The

assistance of Prof. Aurelien Borgoltz and Mr. Tim Meyers over the course of the wind tunnel testing, and the support of the College of Engineering at Virginia Tech in performing that testing, are gratefully acknowledged. Thanks also go to Mr. Daniel Grohol for his assistance in performing computer aided design of the trailing edge treatments, and Mr. Scott Patrick for his help with their manufacture. The support of AVEC Incorporated in providing the phased array system and related assistance is gratefully acknowledged.

The authors would like to sincerely acknowledge the late Professor Geoffrey Lilley, whose long-standing interest in and insight into the aeroacoustics of the owl has been a source of great inspiration.

References

[1] Graham, R. R., "The silent flight of owls," *Journal of the Royal Aeronautical Society*, Vol. 38, 1934, pp. 837-843.

[2] Kroeger, R. A., Gruschka, H. D., and Helvey, T. C., "Low speed aerodynamics for ultra-quiet flight," *Tech. Rep.* AFFDL-TR-71-75, Air Force Flight Dynamics Laboratory, Wright-Patterson AFB, 1972.

[3] Sarradj, E., Fritzsche, C., Geyer, T., "Silent owl flight: bird flyover noise measurements," *AIAA Journal*, Vol. 49(4), 2011, pp. 769-779.

[4] Geyer, T., Sarradj, E., Fritzsche, C., "Measurement of the noise generation at the trailing edge of porous airfoils," *Experiments in Fluids*, Vol. 48(2), 2010, pp. 291-308.

[5] Jaworski, J. W. and Peake, N., "Aerodynamic noise from a poroelastic edge with implications for the silent flight of owls," *Journal of Fluid Mechanics*, Vol. 723, 2013, pp. 456-479.

[6] Jaworski, J. W. and Peake, N., "Parametric guidance for turbulent noise reduction from poroelastic trailing edges and owls," *Proceedings of the19th AIAA/CEAS Aeroacoustics Conference*, Berlin, Germany, 27-29th May 2013, AIAA-2013-2007.

[7] Clark, I. A., Devenport, W. J., Jaworski, J. W., Daly, C., Peake, N. and Glegg, S., "The Noise Generating and Suppressing Characteristics of Bio-Inspired Rough Surfaces", *Proceedings of the AIAA/CEAS 20th Aeroacoustics Conference*, Atlanta, GA, 16-20th June 2014. AIAA-2014-2911.

[8] Glegg, S. and W. Devenport, "The far-field sound from rough-wall boundary layers." *Proceedings of the Royal Society A: Mathematical, Physical and Engineering Sciences*, Vol. 465, 2009, pp. 1717-1734.

[9] Choi, K., and Simpson, R.L., "Some Mean Velocity, Turbulence and Unsteadiness Characteristics of the VPI & SU Stability Wind Tunnel," Department of Aerospace and Ocean Engineering, Virginia Polytechnic Institute and State University, Blacksburg, Virginia 24061, Report VPI-Aero-161, 1987.

[10] Devenport, W. J., Burdisso, R. A., Borgoltz, A., Ravetta, P. A., Barone, M. F., Brown, K. A. and Morton, M. A., "The Kevlar-walled anechoic wind tunnel", *Journal of Sound and Vibration*, vol. 332(17), 2013, pp. 3971-3991.

[11] Walsh, M. J., "Riblets as a Viscous Drag Reduction Technique", *AIAA Journal*, vol. 21(4), 1983, pp. 485-486.

[12] Choi, H., Moin, P., and Kim, J., "Direct numerical simulation of turbulent flow over riblets", *Journal of Fluid Mechanics*, vol. 255, 1993, pp. 503-539.

[13] Sijtsma, P., "CLEAN based on spatial source coherence", *Aeroacoustics*, vol. 6(4), 2007, pp. 357-374.

[14] Drela, M., "XFOIL: An analysis and design system for low Reynolds number airfoils," 1989.

Tables

Table 1 Freestream turbulence levels

Freestream Velocity, U_∞ (m/s)	RMS Streamwise Fluctuations, u'/ U_∞
12	0.016%
21	0.021%
30	0.024%
48	0.029%
57	0.031%

Table 2 List of finlet cases and dimensions in millimeters.

Config No.	Height	Spacing[1]	Thickness/Rail Diameter	TE Extension	Substrate	Suction Only
Control Cases						
C0	-	-	-	-	-	-
C1	-	-	-	-	0.5	-
C2	-	-	-	-	0.75	-
Fence Cases						
F0	4	4	0.5	10	0.5	-
F1	4	1	0.5	0	0.5	-
F2	4	1	0.5	10	0.5	-
F3	4	6	0.5	10	0.75	-
F4	4	10	0.5	10	0.5	-
F5	2	1	0.5	10	0.75	-
F6[2]	4	1	0.5	10	0.5	-
F7[3]	4	1	0.5	10	0.75	-
F8	8	4	0.5	10	0.5	-
F9	4	4	2	10	0.75	-
F1S	4	1	0.5	0	0.5	Y
F2S	4	1	0.5	10	0.5	Y
F8S	8	4	0.5	10	0.5	Y
F10S	16	4	0.5	0	0.5	Y
Rail Cases						
R0	4	2.5	1.25	10	0.75	-
R1	4	2.5	1.25	0	0.75	-
R2	8	2.5	1.25	10	0.75	-
R3	4	5	2.5	10	0.75	-
R4	8	10	1.25	10	0.75	-
R5[2]	4	2.5	1.25	10	0.75	-

[1] Spacing was measured as the width of the open gaps between the finlets, not as the center-to-center spacing of the finlets. This preserves the spacing parameter when varying finlet thickness/diameter.

[2] Fence/rail length upstream of the trailing edge varied periodically in the spanwise direction with one period being the sequence 101.6mm, 12.7mm, 25.4mm, 12.7mm, 50.8mm, 12.7mm, 25.4mm, and 12.7mm.

[3] Fence length upstream of the trailing edge varied periodically as in configuration 6, but with fence height scaled to 4mm, 2.5mm, 3mm, 2.5mm, 3.5mm, 2.5mm, 3mm, and 2.5mm in the same periodic sequence, respectively.

Table 3 Overall sound levels (dB) in the frequency range of 1500 – 5000 Hz.

Config No.	Angle of Attack			
	-2.5 deg	-0.5 deg	3.0 deg	6.9 deg
Control Cases				
C0	57.3	55.8	53.8	54.6
C1	58.2	56.5	54.0	54.5
C2	58.4	57.2	54.4	54.7
Fence Cases				
F0	53.3	53.0	52.2	54.1
F1	52.0	51.3	51.6	54.0
F2	50.3	50.4	51.0	54.0
F3	54.0	53.6	52.5	53.8
F4	54.7	54.2	53.2	54.6
F8	51.9	51.6	51.5	53.6
F9	52.8	52.4	52.0	53.7
F8S	54.7	53.3	51.7	53.3
Rail Cases				
R0	53.4	52.8	51.8	53.3
R1	53.3	52.6	52.2	53.8
R2	53.2	52.3	51.6	53.4
R3	53.4	53.1	52.6	54.5

Figures

Fig. 1 Close-up view of a flight feather of a great gray owl (Strix nebulosa) showing the canopy structure formed by the hairs.

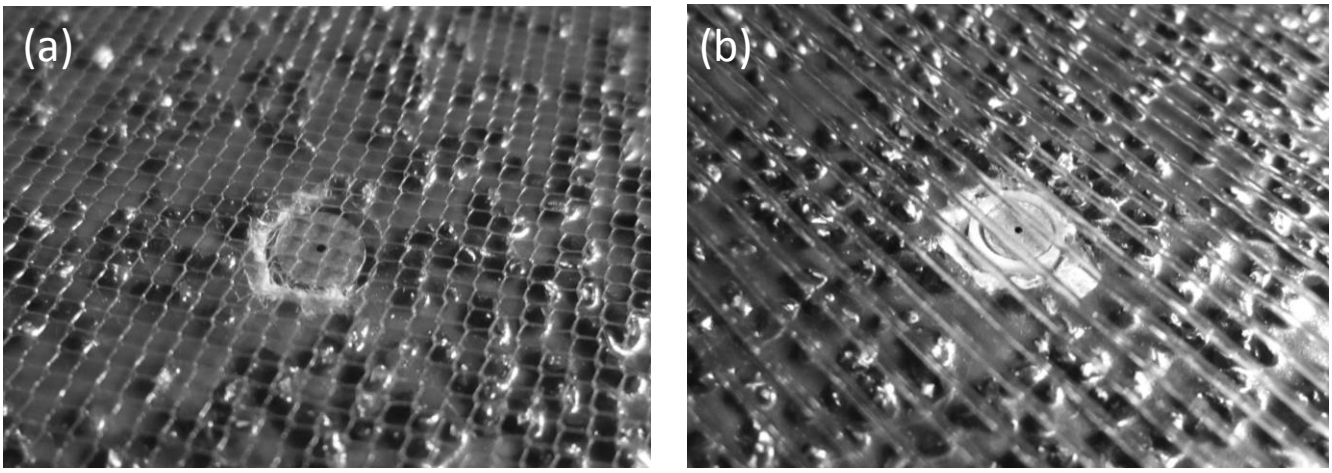

Fig. 2 Example fabric canopy arrangements studied in the wind tunnel, shown shrouding a sandpaper type rough surface. (a) Commercial wedding-veil type fabric with multi-directional fibers. (b) Custom designed unidirectional fiber fabric with fibers oriented only in the flow direction.

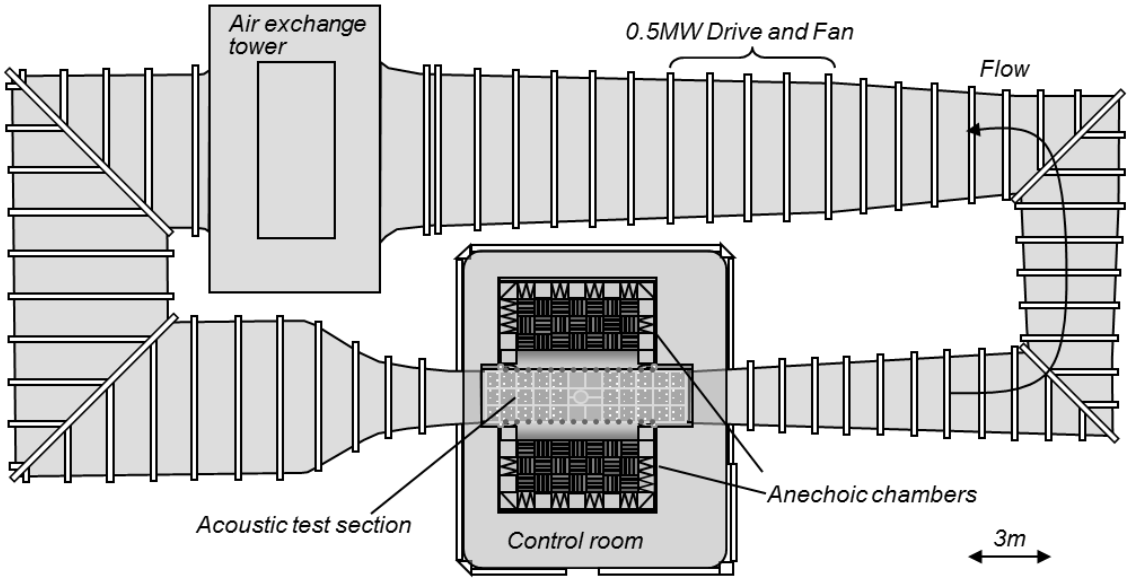

Fig. 3 Plan view schematic of the Virginia Tech Stability Wind Tunnel in anechoic configuration.

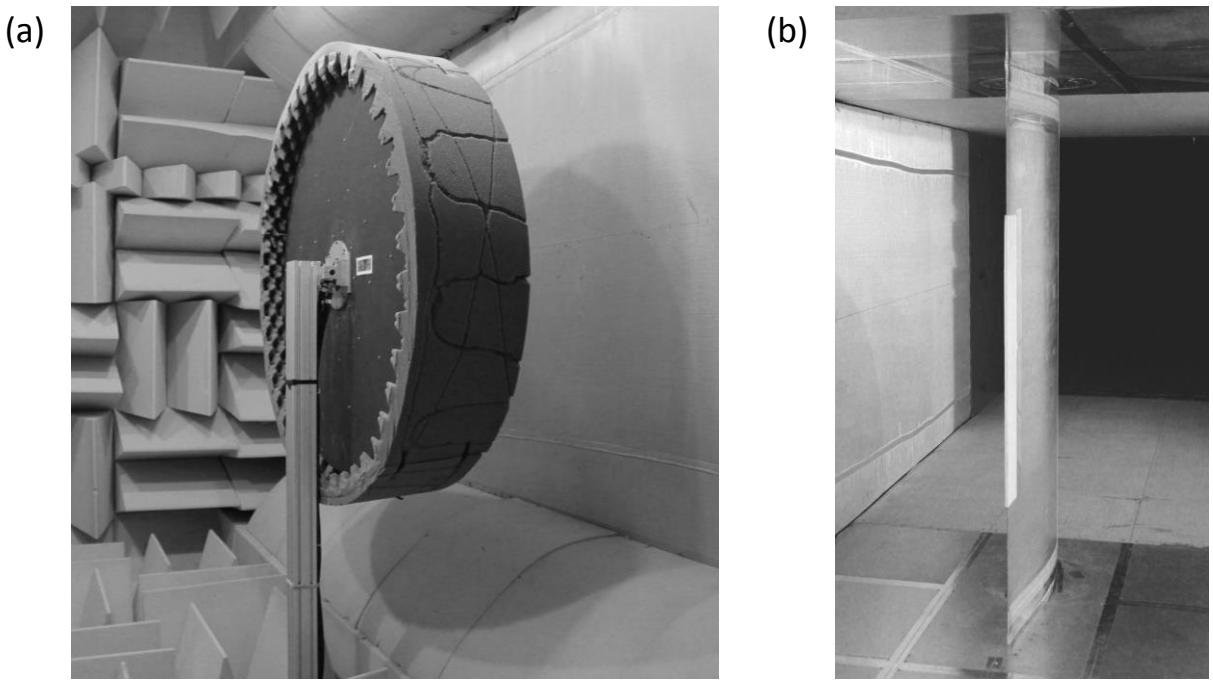

Fig. 4 (a) The 117-microphone phased array system installed in the port-side anechoic chamber directed at the suction side of (b) the 0.8-m chord DU96-W180 airfoil mounted in the anechoic test section.

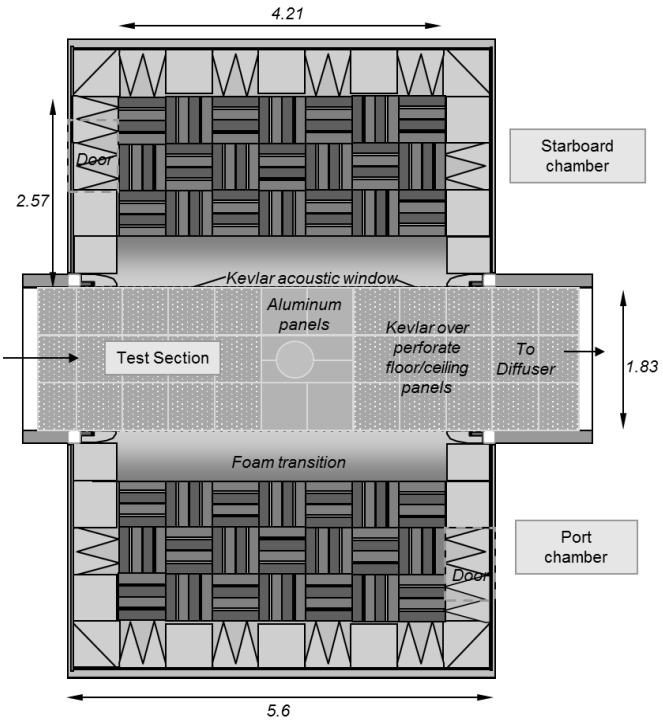

Fig. 5 Plan view cross-section of the anechoic system as installed showing the test section flanked by the two anechoic chambers. Dimensions in meters.

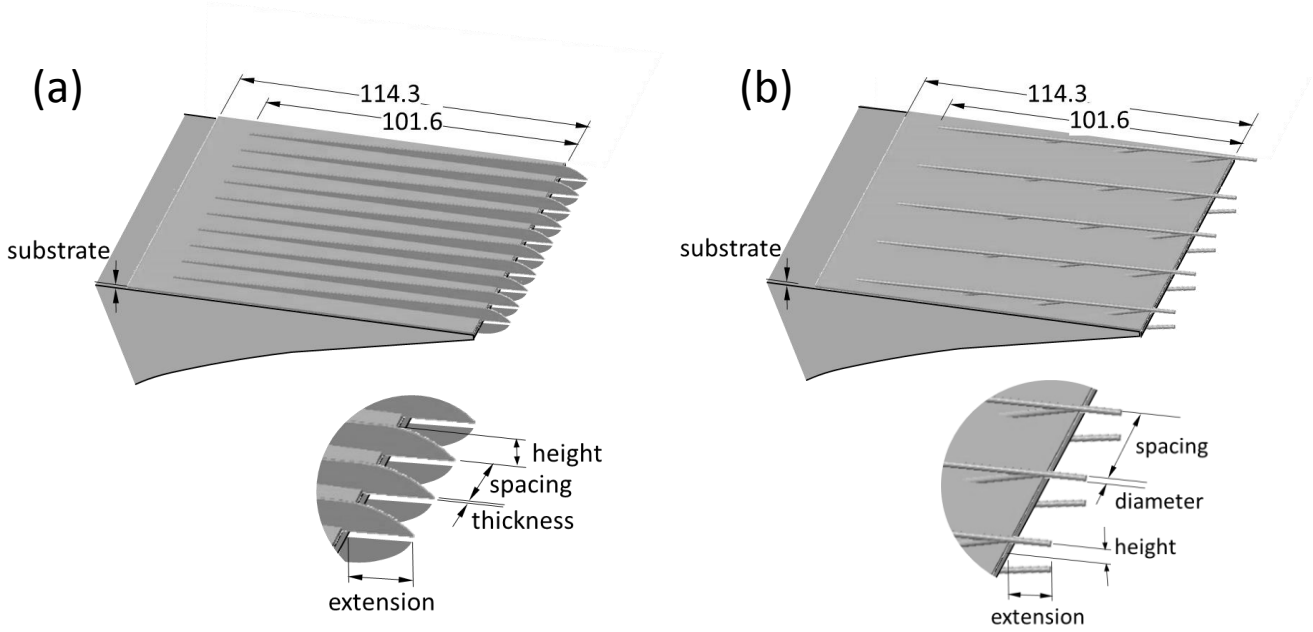

Fig. 6 Treatment designs tested on the DU96-W180. (a) Finlet fence, (b) finlet rail. Diagrams show finlets attached to the trailing edge portion of the airfoil. Dimensions in millimeters.

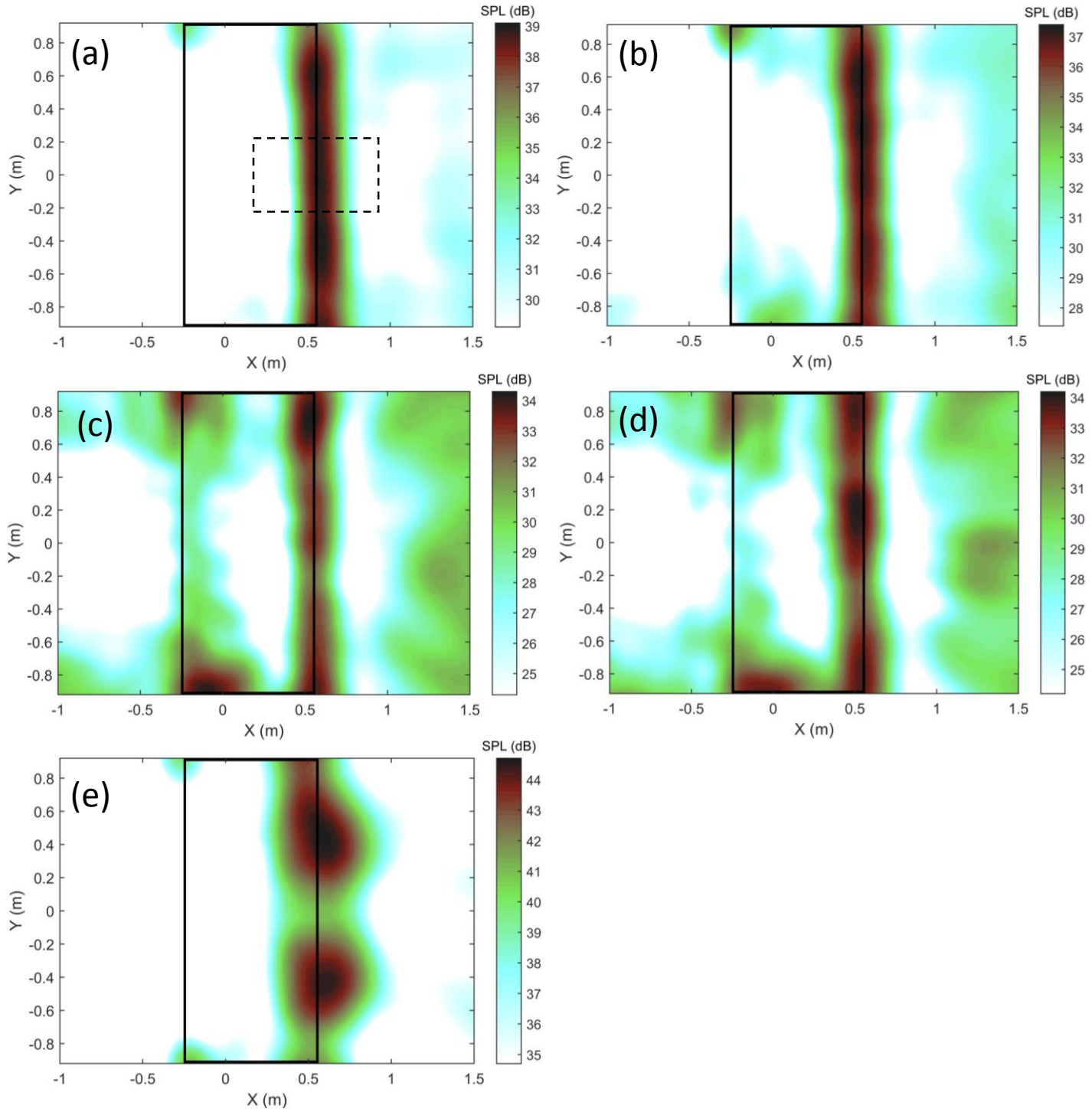

Fig. 7 Beamform maps showing the trailing edge noise radiated by the untreated DU96-W180 airfoil at 3 kHz at angles of attack of (a) -2.5, (b) -0.5, (c) 3.0, (d) 6.9, and (e) 14.8 degrees. Re=3 million.

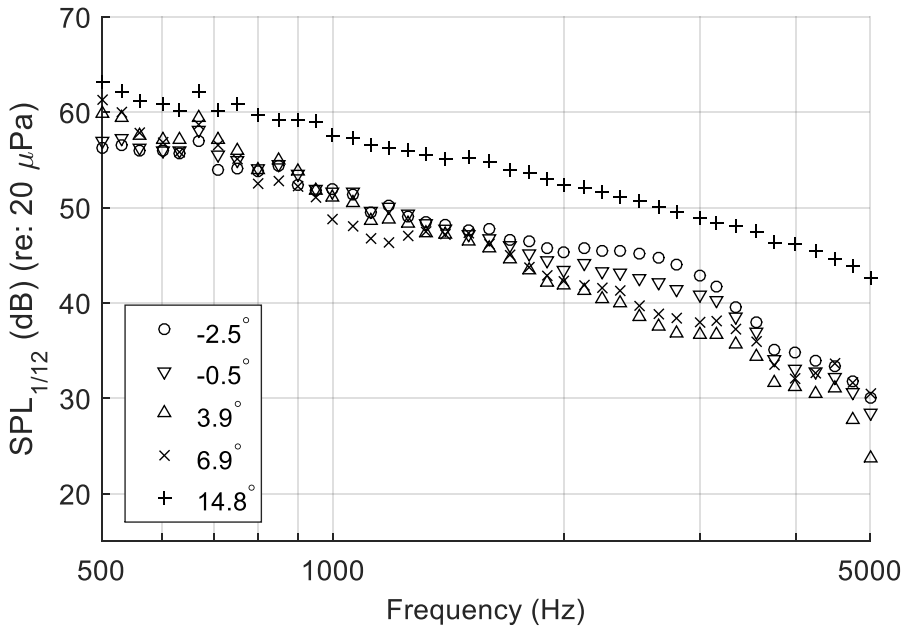

Fig. 8 Noise spectra for the untreated DU96-W180 at Re=3 million, as a function of angle of attack obtained by integrating phased array results over the central 25% of the airfoil span, as indicated by the dashed region in Fig. 7a.

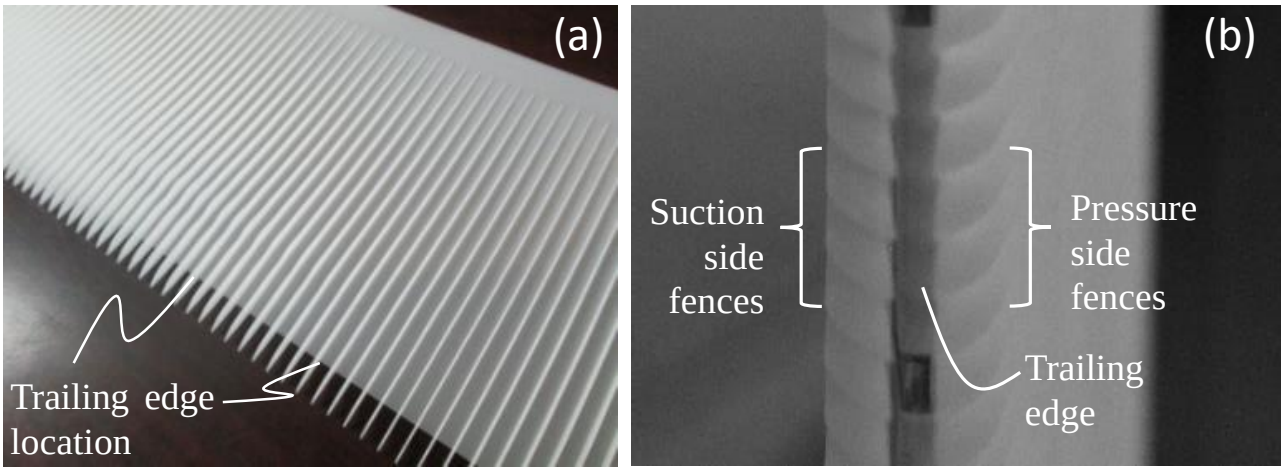

Fig. 9 Finlet configuration F0. (a) Before attachment to the airfoil. (b) After attachment to both sides of the airfoil (view seen looking upstream at the trailing edge). Note the gap between the fence extensions on either side of the trailing edge.

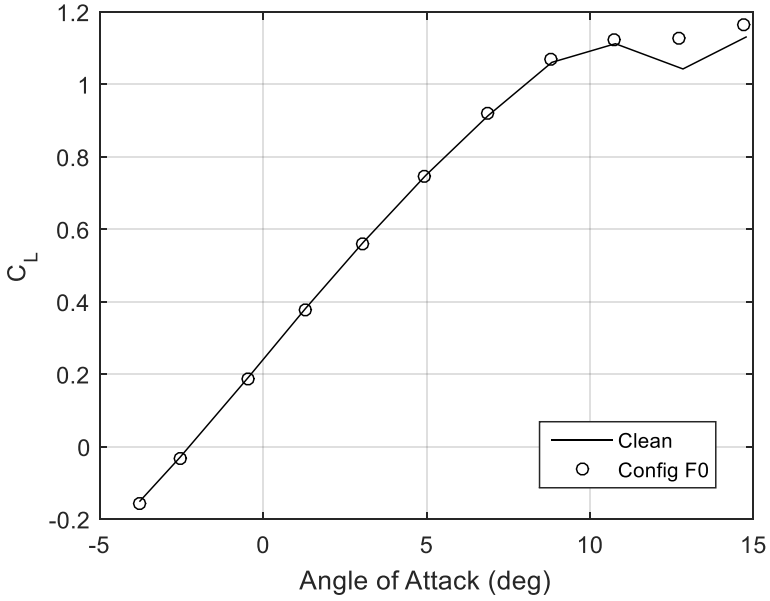

Fig. 10 Lift coefficient plotted against angle of attack for the untreated ('Clean') and baseline treated ('Config 5') DU96-W180 at Re=3 million.

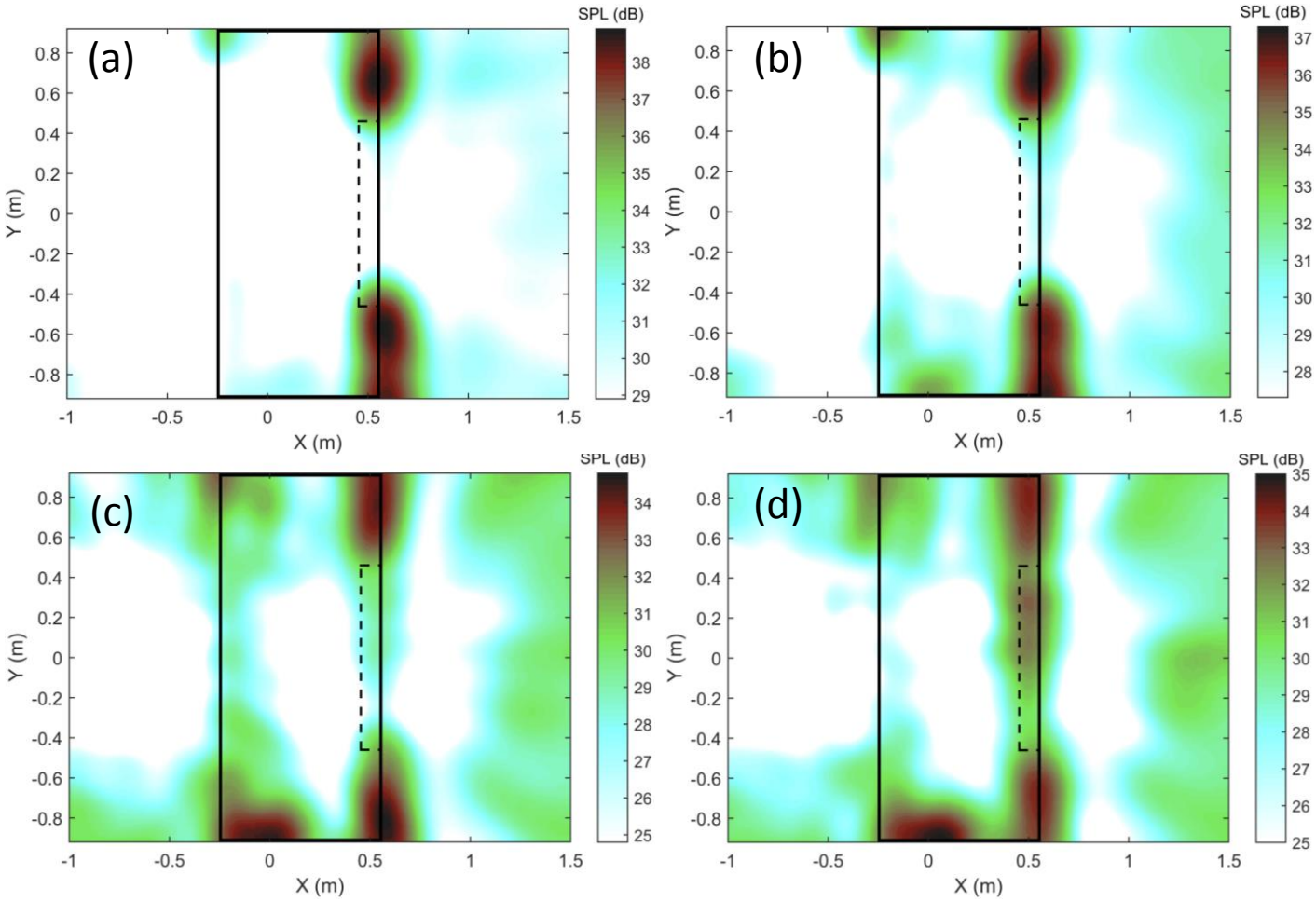

Fig. 11 Beamform maps showing the trailing edge noise radiated by the DU96-W180 at 3 kHz at angles of attack of (a) -2.5, (b) -0.5, (c) 3.0, and (d) 6.9 degrees with the baseline (configuration F0) treatment applied across the central half span (as indicated by the dashed rectangle). Re=3 million.

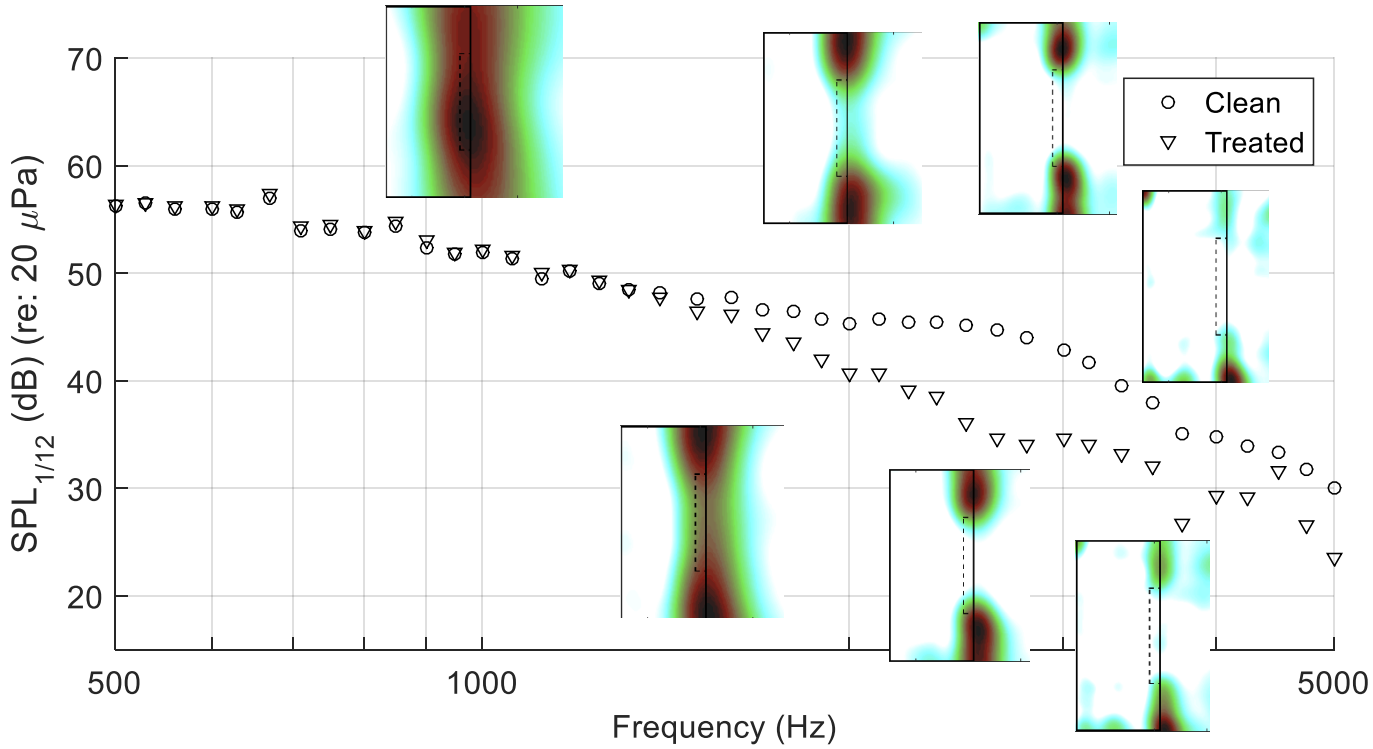

Fig. 12 Noise spectra for configuration F0 treatment compared to results for the clean case. Re=3 million, -2.5 degrees angle of attack. Inset images show beamform maps of the treated airfoil noise to illustrate the blurring effects of the large spot size at frequencies below about 2 kHz.

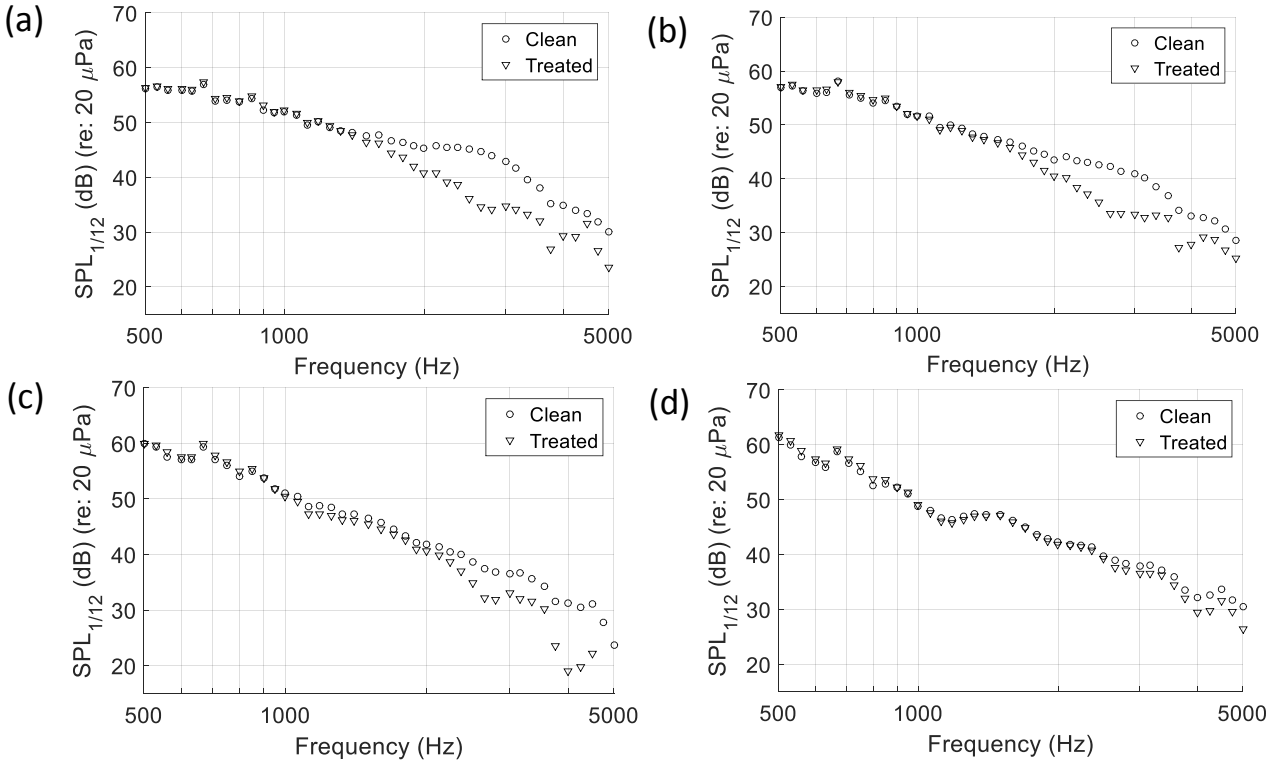

Fig. 13 Noise spectra (in SPL re 20 μPa) for configuration F0 treatment compared to results for the clean case at angles of attack of (a) -2.5 (b) -0.5 (c) 3.0 and (d) 6.9 degrees. Re=3 million.

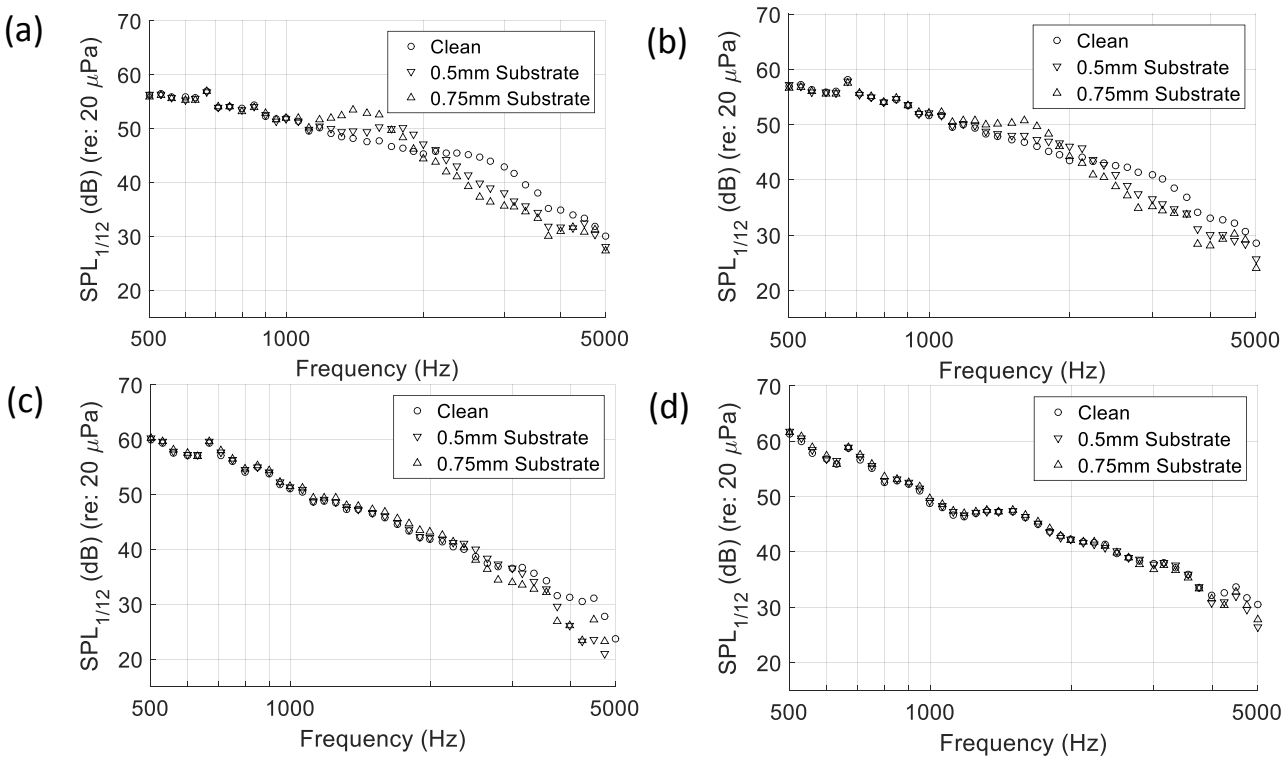

Fig. 14 Noise spectra (in SPL re 20 μPa) for configurations C1 and C2 showing substrate-alone effects at angles of attack of (a) -2.5 (b) -0.5 (c) 3.0 and (d) 6.9 degrees compared to the clean case. Re=3 million.

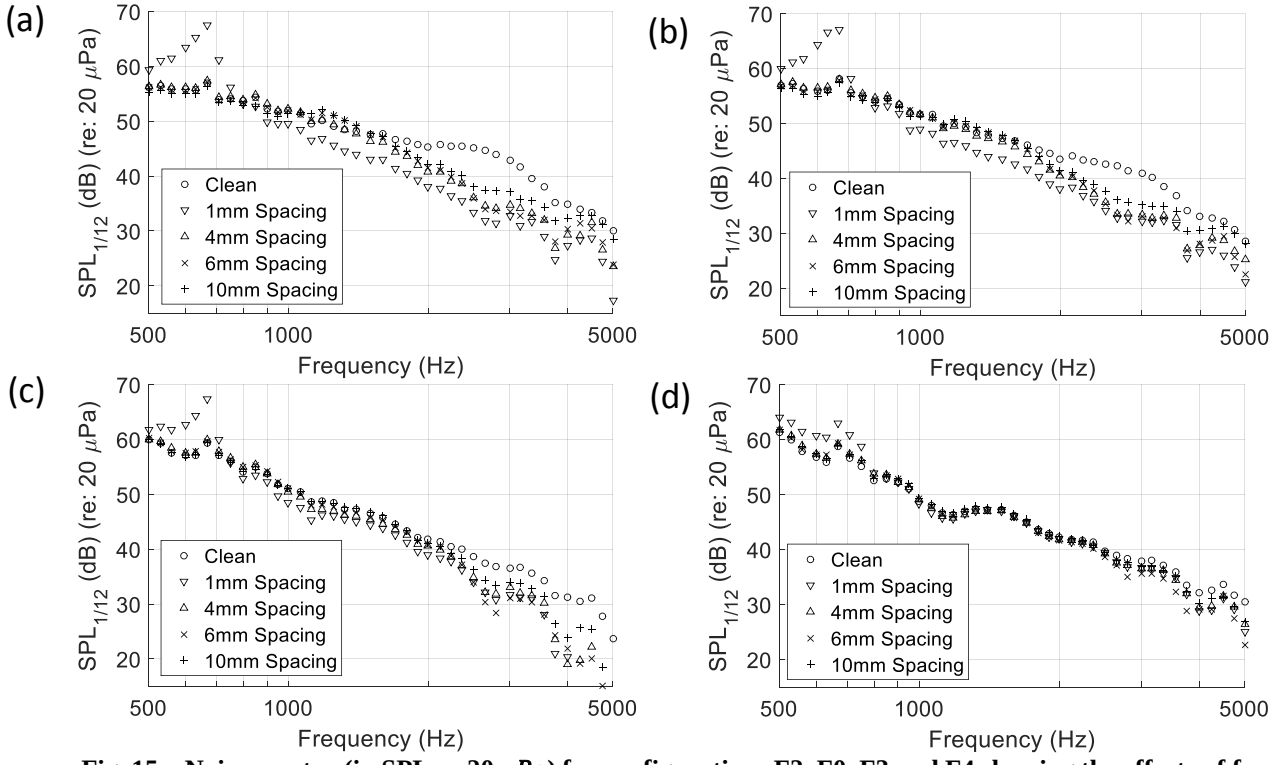

Fig. 15 Noise spectra (in SPL re 20 μPa) for configurations F2, F0, F3 and F4 showing the effects of fence spacing on noise radiation at angles of attack of (a) -2.5 (b) -0.5 (c) 3.0 and (d) 6.9 degrees compared to the clean case. Re=3 million.

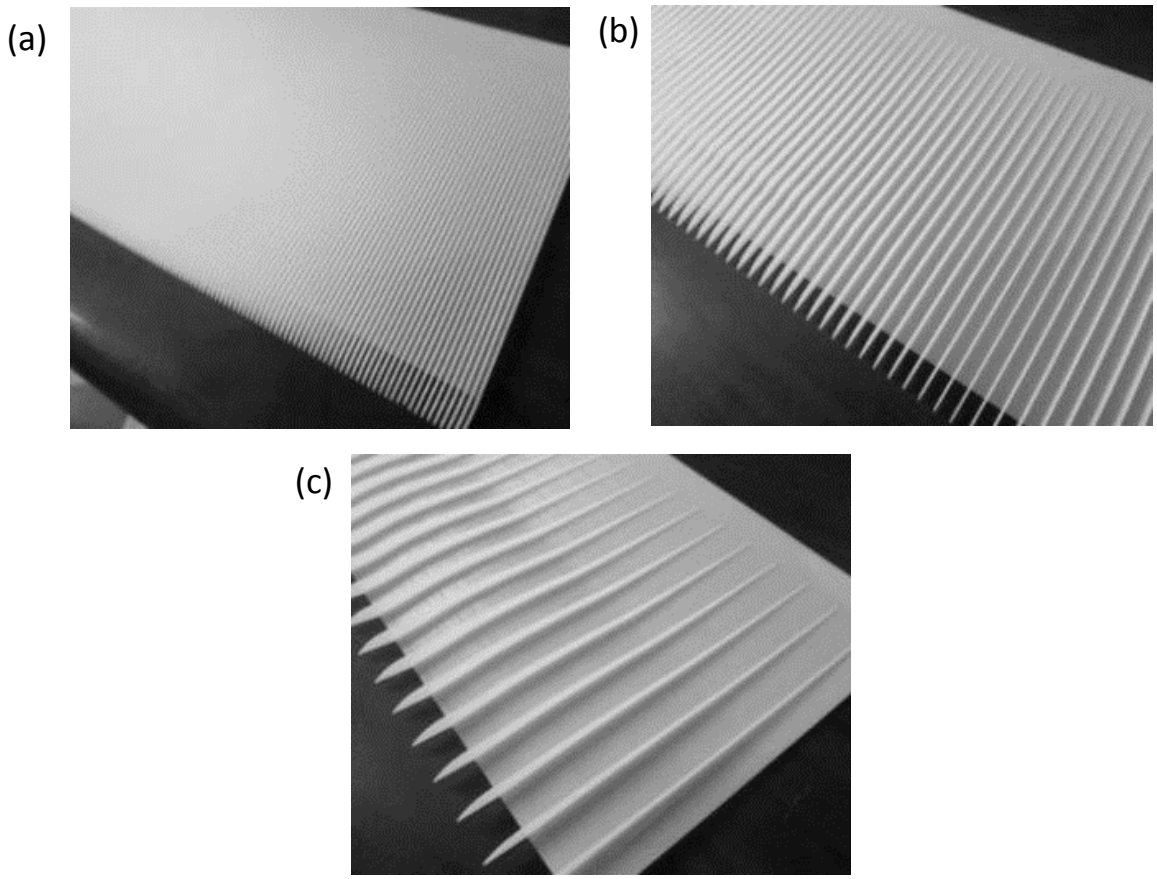

Fig. 16 Photographs of treatments F2, F0 and F4, fence treatments with (a) 1mm, (b) 4mm, and (c) 10mm spacing respectively, before application to the airfoil.

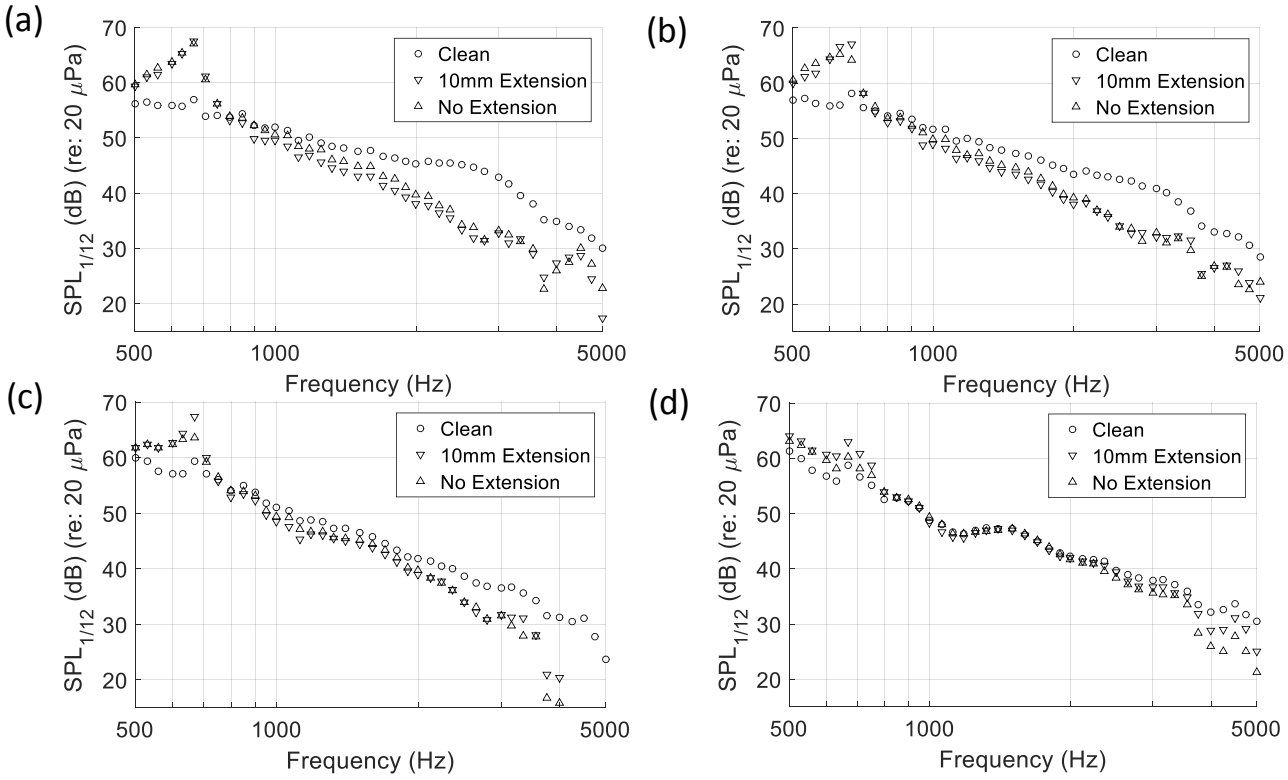

Fig. 17 Noise spectra (in SPL re 20 μPa) for configurations F2 and F1 showing the effects of fence extension over the trailing edge on noise radiation at angles of attack of (a) -2.5 (b) -0.5 (c) 3.0 and (d) 6.9 degrees compared to the clean case. Re=3 million.

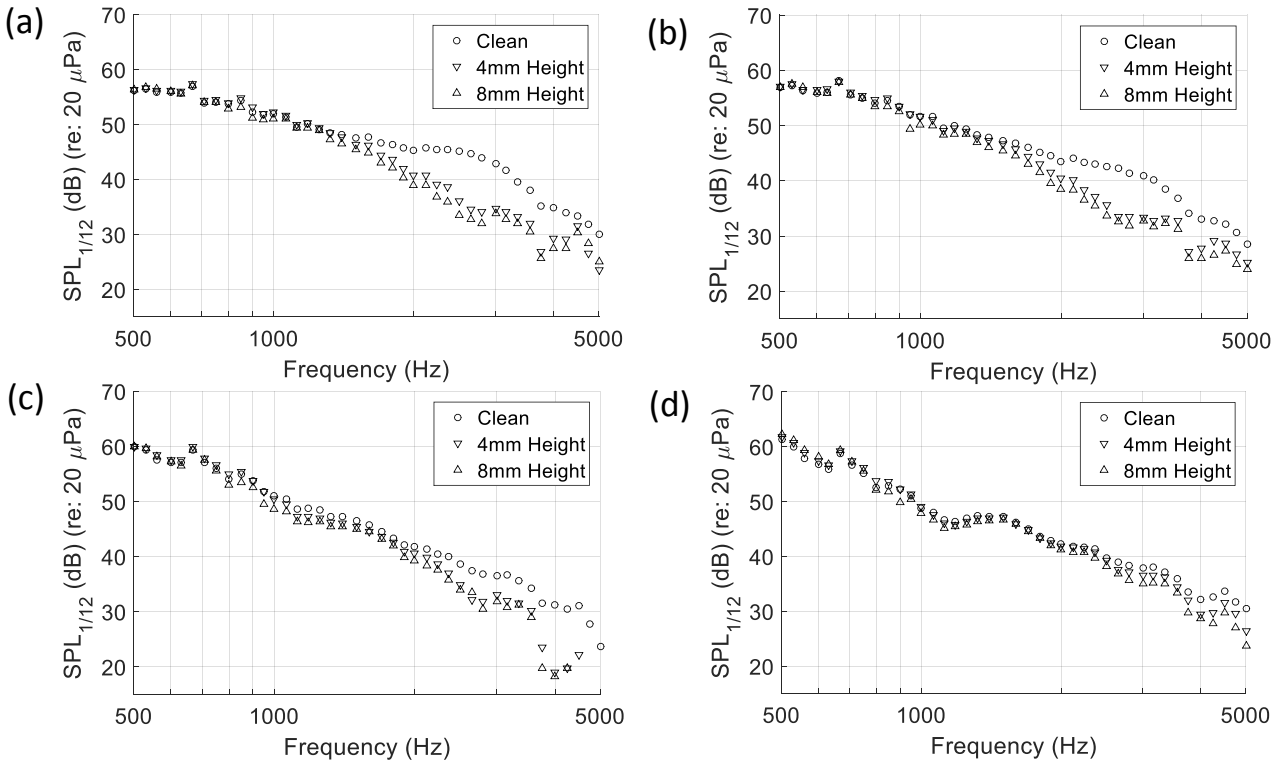

Fig. 18 Noise spectra (in SPL re 20 μPa) for configurations F0 and F8 showing the effects of fence height on noise radiation at angles of attack of (a) -2.5 (b) -0.5 (c) 3.0 and (d) 6.9 degrees compared to the clean case. Re=3 million.

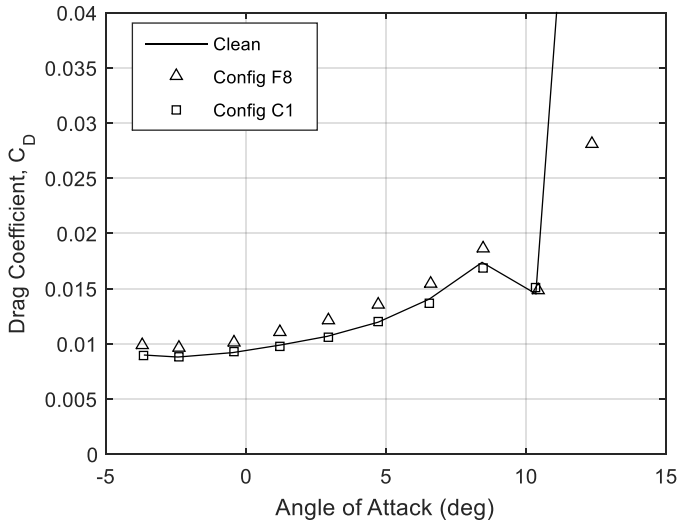

Fig. 19 Drag coefficient as a function of angle of attack measured for the clean airfoil, with configuration F8, and with the substrate alone (configuration C1). Re=3 million.

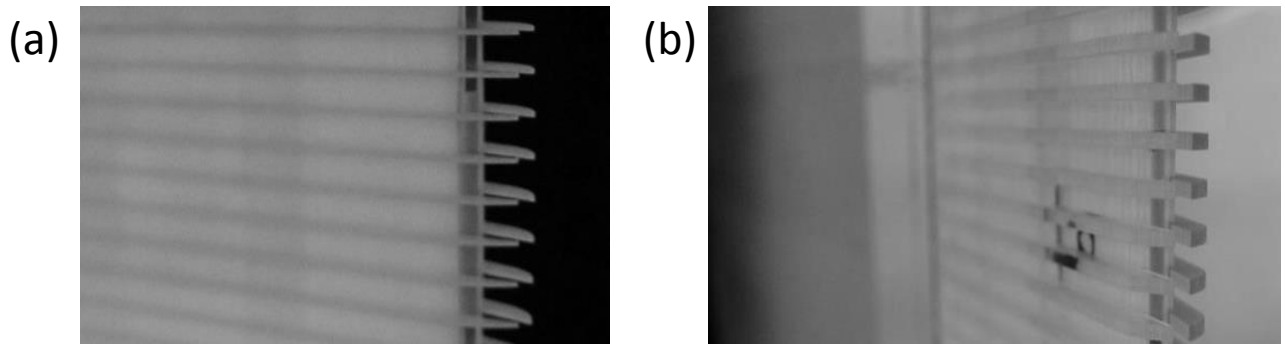

Fig. 20 Comparison of configurations (a) F0 and (b) F9 illustrating the difference in fence thickness. Pictures are looking upstream from the trailing edge.

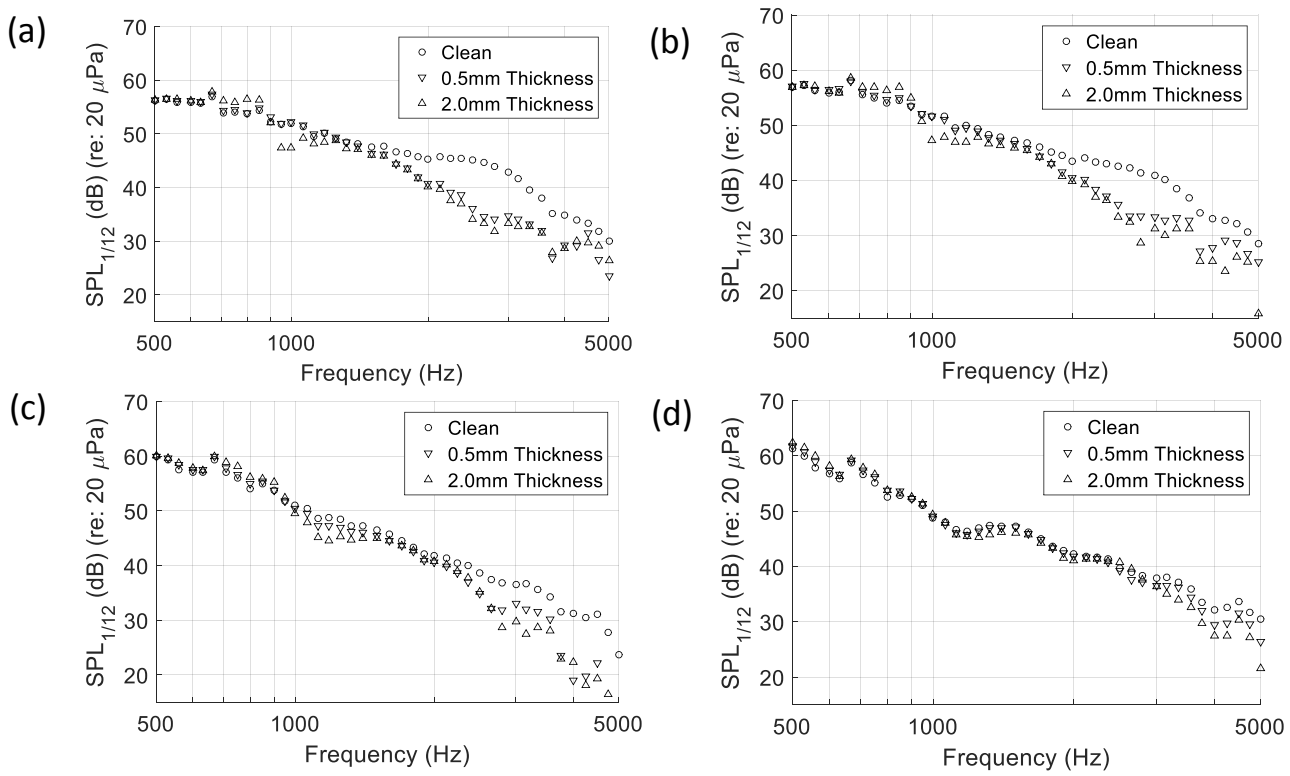

Fig. 21 Noise spectra (in SPL re 20 μPa) for configurations F0 and F9 contrasting the effects of fence thickness at angles of attack of (a) -2.5 (b) -0.5 (c) 3.0 and (d) 6.9 degrees compared to the clean case. Re=3 million. Note that configurations F0 and F9 have different substrate thicknesses of 0.5 mm and 0.75 mm, respectively.

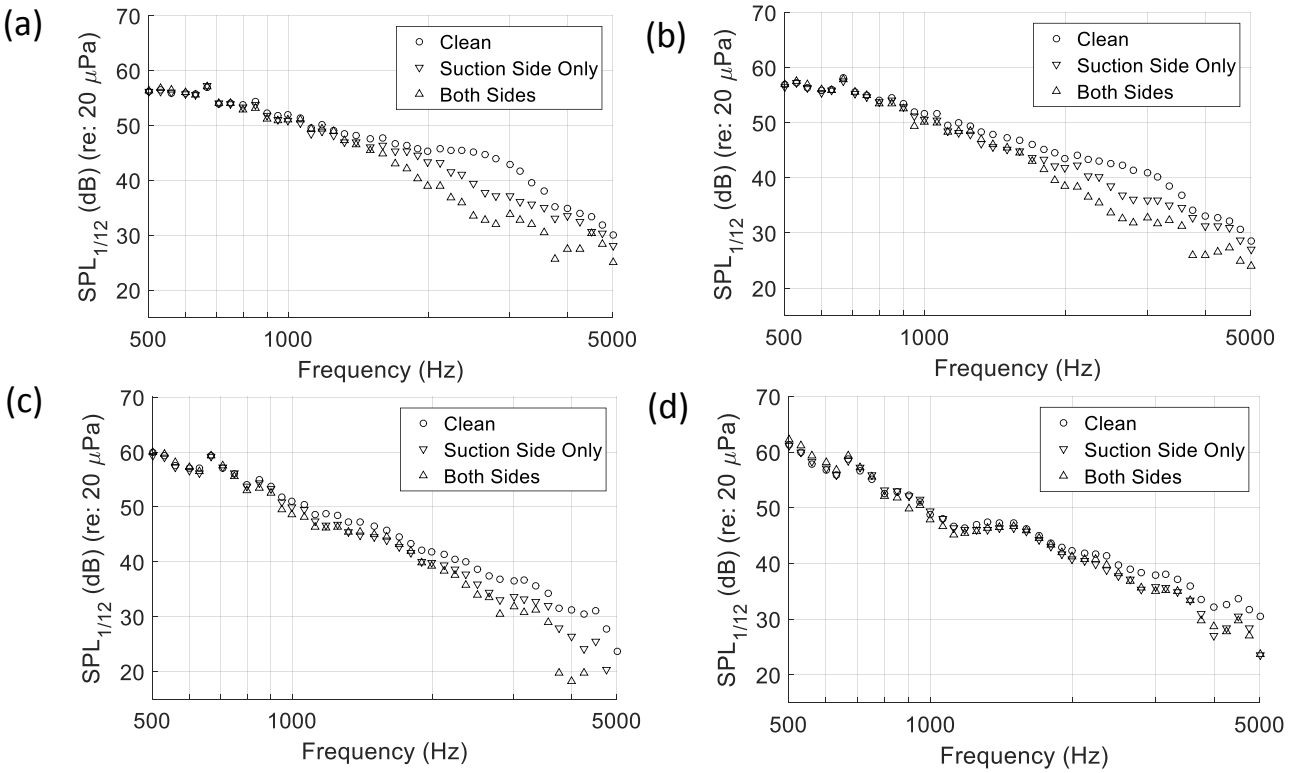

Fig. 22 Noise spectra (in SPL re 20 μPa) for configurations F8 and F8S contrasting the effects of applying the treatment to both sides of the airfoil (F8) and just the suction side (F8S), at angles of attack of (a) -2.5 (b) -0.5 (c) 3.0 and (d) 6.9 degrees, compared to the clean case. Re=3 million.

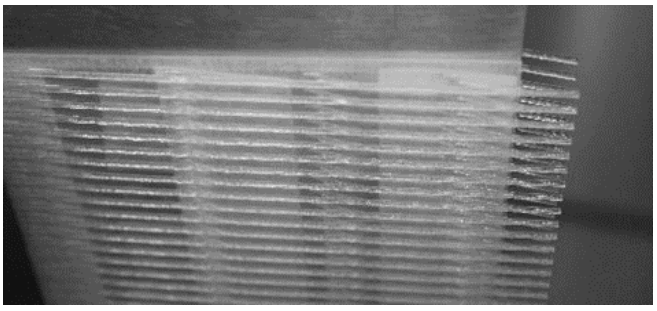

Fig. 23 Side view of configuration R0 applied to both sides of the airfoil, showing the rail geometry.

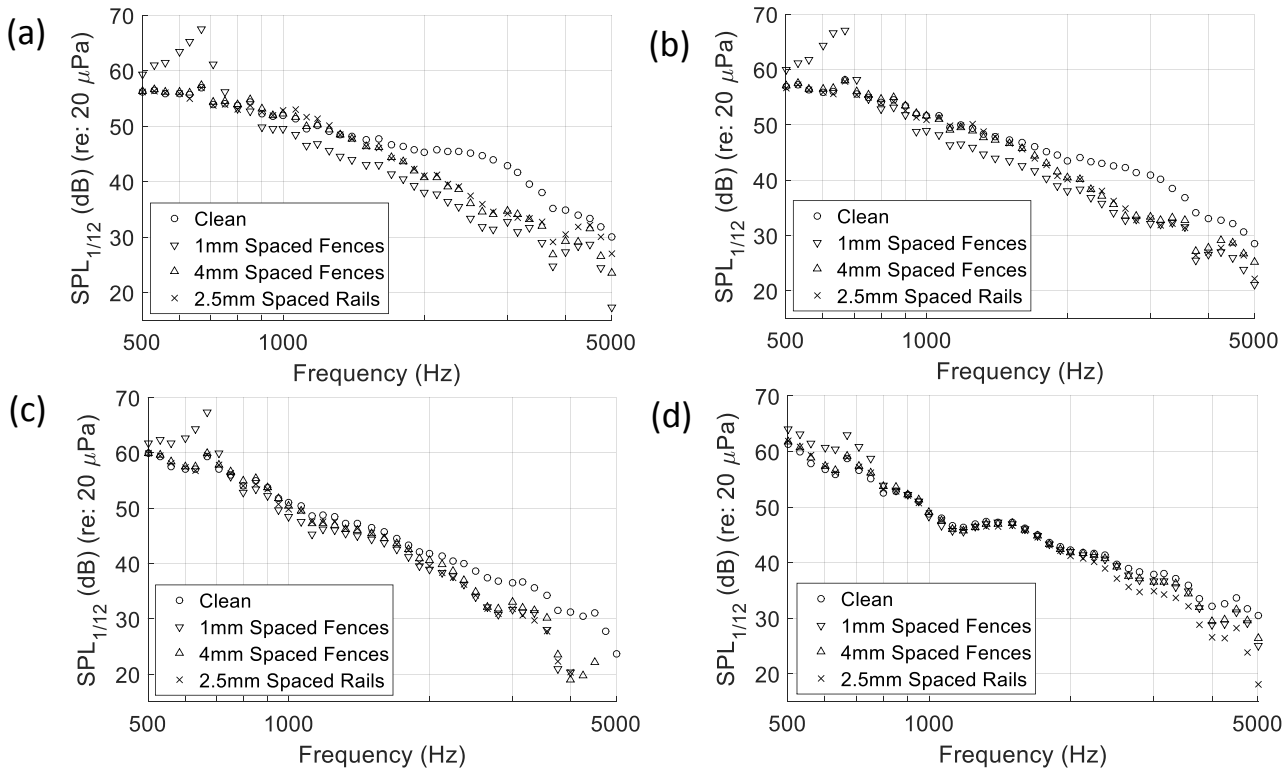

Fig. 24 Noise spectra (in SPL re 20 μPa) for configurations F2, F0 and R0 contrasting the effects of fence and rail treatments of similar scale, at angles of attack of (a) -2.5 (b) -0.5 (c) 3.0 and (d) 6.9 degrees, compared to the clean case. Re=3 million.

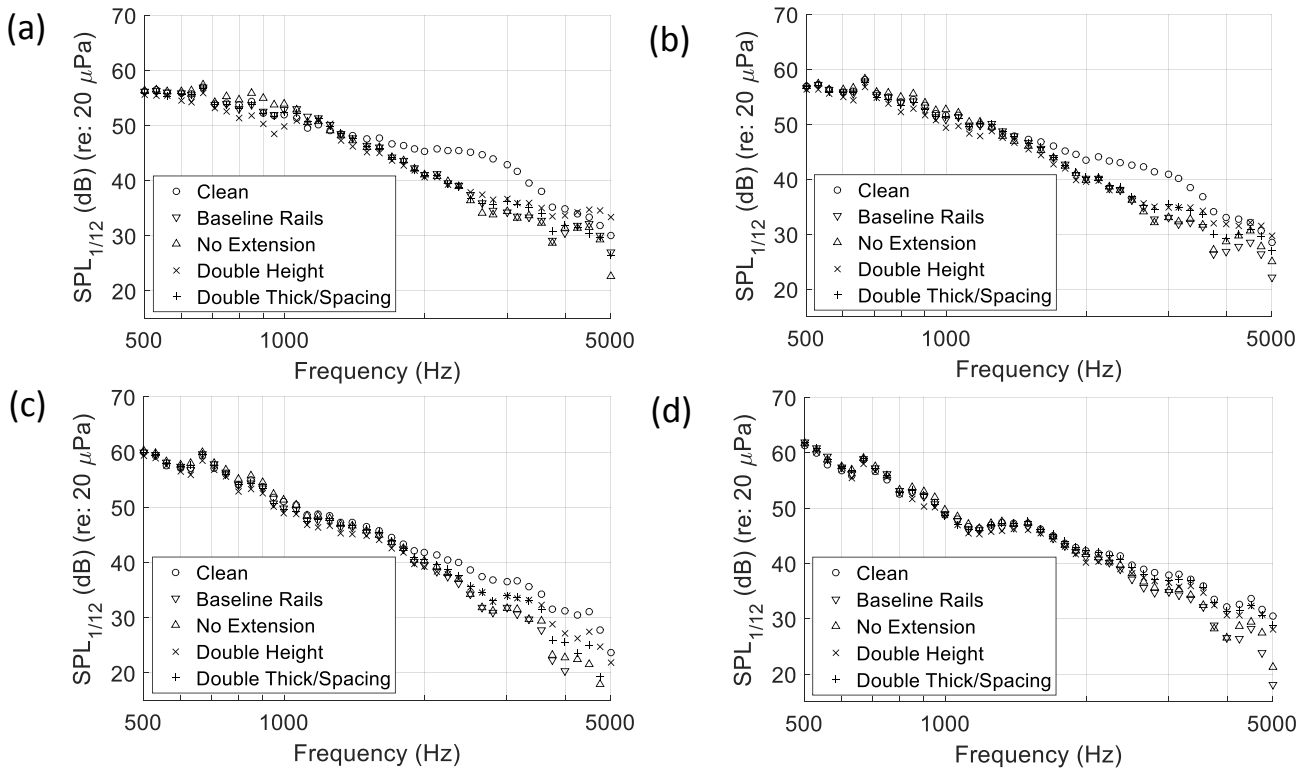

Fig. 25 Noise spectra (in SPL re 20 μPa) for configurations R0, R1, R2 and R3 contrasting the effects of different rail treatments, at angles of attack of (a) -2.5 (b) -0.5 (c) 3.0 and (d) 6.9 degrees, compared to the clean case. Re=3 million.